



UNIVERSITÀ DEGLI STUDI DI PADOVA

Dipartimento di Fisica e Astronomia “Galileo Galilei”

Department of Physics, Leiden University

Master Degree in Physics

Final Dissertation

Squeezing Optomechanics

Thesis supervisor:

Prof. Giovanni Mattei

Thesis co-supervisor:

Prof. Dirk Bouwmeester

Candidate:

Matteo Fiscaro

Academic Year 2018/2019

Contents

Abstract	2
1 Fiber to cavity coupler for Cryogenic applications	4
1.1 The ray transfer matrix method for Gaussian beams	5
1.2 Finding the optimal lenses configuration	7
1.3 Behaviour of the system at cryogenic temperatures	9
1.4 Results of the simulations	10
1.5 Experiment: testing the concept of the design	12
1.6 Conclusions and future developments	19
2 Pound-Drever-Hall laser frequency stabilization	21
2.1 The general idea	22
2.2 Quantitative explanation	22
2.2.1 Reflection of a monochromatic beam from a Fabry-Perot cavity	22
2.2.2 Beam modulation: sidebands	24
2.2.3 The error signal	24
2.3 The role of reflection	26
2.4 Simulations	28
2.5 Experimental verification	31
2.6 Conclusions	34
3 Decay of a thermomechanical squeezed state	35
3.1 Mathematical description of squeezing	35
3.2 The Membrane	38
3.3 Basics of the Optomechanical interaction	40
3.3.1 Mechanical resonators	40
3.3.2 Light inside the cavity	41
3.3.3 Coupling of light with the mechanical oscillator	41
3.4 Optical setup	45
3.5 Experiment and data analysis	47
3.6 Conclusions and future developments	52

Abstract

Optomechanics studies the interaction between light and a mechanical resonator, enabled via radiation pressure. Employing a high finesse cavity it is possible to enhance this interaction, enabling the possibility of bringing macroscopic objects in a quantum superposition of states and possibly opening the way to the experimental study of quantum decoherence. The work carried out in this thesis consists in the development and improvement of an experimental setup used to perform optomechanics experiment, that in the future will allow to experimentally investigate the foundations of quantum mechanics.

The first part of this thesis deals with the development of an optical system for cryogenic applications that matches the Gaussian mode of a SM optical fiber into a high Finesse optical cavity. We will discuss how a prototype has been designed and experimentally tested.

In the second section will be investigated a technical problem encountered in the Pound-Drever-Hall (PDH) frequency stabilization setup implemented using optical fibers instead of free space optics. The presence of some wiggles in the PDH error signal, and a time dependent shift of its baseline makes difficult to lock the laser to the cavity for a sufficient amount of time to perform experiments. Numerical simulations and experiments will be performed in order to understand the origin of the problem, and to solve it.

The last part of this work consists in the experimental study of the decay of a thermomechanical squeezed state, a phenomenon that to the knowledge of the author has never been investigated yet. In particular we will create a thermal squeezed state by parametric modulation of the spring constant, and we will study its time evolution after we switch off this parametric modulation.

1 Fiber to cavity coupler for Cryogenic applications

Around the world there are different research groups involved in optomechanical experiments, each one of them using a different configuration (different type of mechanical resonator and cavity). A review of the state of the art can be found in [1]. The Bouwmesteer group is focusing on a system in which a high Q mechanical resonator (a SiN membrane with dimensions of $3mm \times 3mm \times 25nm$) is placed in the middle of high finesse Fabry-Perot cavity, which is made of high reflectivity spherical mirrors (radius of 50mm) placed at a distance $L=94$ mm with respect to each other. The cavity is suited for a wavelength $\lambda = 1064nm$ and has a Finesse $F=19000$. With this setup it is possible to investigate optomechanical effects in the quantum regime, by placing the cavity inside a dilution refrigerator. This cryostat doesn't have any window that connect it with the outside, and therefore light is sent into the cavity through optical fibers. For this reasons, the optical elements that perform the mode matching between the SM optical fiber and the cavity are also placed inside the cryostat, and are cooled down during the process. The change in temperature affects dramatically the properties of these optical components, and as a result if one doesn't counteract the effect, the coupling between the optical fiber and the cavity at low temperature will be very low or not present at all, even when starting with a high value at room temperature. In the past the Bouwmesteer group has already performed experiments at cryogenic temperatures, relying on a fiber to cavity coupling system that included piezos and motors to move the optical components during the cooling down, in order to be able to compensate for the change in the optical and mechanical properties of the components. This design has some drawbacks, for example the setup was mechanically not rigid enough, and in the cryostat it was shaking so much that the PDH lock couldn't be established. The other main disadvantage is that this scheme requires an operator that controls the active elements to re-adjust the positions of the optical components during the cool down of the system, which normally takes few days and has to be constantly and closely monitored.

At the moment I joined the research group, this old cryogenic setup had already been dismanteled, in order to move towards a new design for the fiber to cavity coupler that doesn't have the previously mentioned problems. I have been asked to conceptually design (and test) such a system, with the constraint of not employing any active elements to control the optical components: once everything is in place at room temperature, no adjustment should be required to maintain the same coupling (or at least a high value) also at cryogenic temperatures. In order to achieve this purpose one should carefully choose the materials of the setup and its symmetry. The only constraints that we have are the dimensions of the optical

cavity and the radius of curvature of the mirrors, already mentioned before. With this constraint, the design of the optical setup has been chosen according to the following criteria:

- All the optical components will lie on the central axis of a cylinder, in order to minimize the effects of thermal contraction/expansion along the radial direction.
- The material of this cylindrical structure is Invar (a metal alloy composed of 64% of Fe and 36% of Ni), which has a very low coefficient of thermal expansion: the integral coefficient of expansion from 300K to 4K is

$$\frac{\Delta L}{L_0} = -4.0 \times 10^{-4} ,$$

where L_0 is the length at 300K and ΔL is the difference between the length at 4K and the length at 300K.

- The distance between the tip of the optical fiber and the cavity has to be kept as small as possible, in order to minimize the effects of misalignment on the optical components
- The number of lenses used to couple light from the fiber to the cavity has to be kept as low as possible, in order to have the simplest design.

In order to find an optical configuration that couples light into the cavity satisfying these conditions, a Matlab program based on ray transfer matrix for Gaussian beams has been implemented

1.1 The ray transfer matrix method for Gaussian beams

Before describing the propagation of a Gaussian beam through optical components, we need to introduce it. A Gaussian beam is a beam of monochromatic electromagnetic radiation whose transverse magnetic and electric field amplitude profiles are given by the Gaussian function. Moreover it is true that this mode belongs to the so called Hermite-Gaussian modes, a set of modes of the electromagnetic field that can be used to describe an arbitrary field distribution and in particular the field distribution of an electromagnetic wave inside an optical resonator. If we set a reference system in which z is the direction of propagation of light and the x - y plane is the plane orthogonal to the z axis, we can write the electric field of the

Hermite-Gaussian modes as:

$$E_{m,n}(x, y, z) = E_0 \frac{W_0}{W(z)} H_m \left(\frac{\sqrt{2}x}{W(z)} \right) H_n \left(\frac{\sqrt{2}y}{W(z)} \right) \times \exp \left[-\frac{(x^2 + y^2)}{W^2(z)} - ik \frac{(x^2 + y^2)}{2R(z)} - ikz + i(m + n + 1) \arctan \left(\frac{z}{z_0} \right) \right] \quad (1)$$

where m and n indicates the order of the mode, and H are the hermite polynomials. The Gaussian beam is obtained for m=n=0:

$$E_{0,0}(x, y, z) = E_0 \frac{W_0}{W(z)} \times \exp \left[-\frac{(x^2 + y^2)}{W^2(z)} - ik \frac{(x^2 + y^2)}{2R(z)} - ikz + i \arctan \left(\frac{z}{z_0} \right) \right] \quad (2)$$

In this case the parameter R gives the radius of curvature of the wavefront of the beam, at the coordinate z:

$$R(z) = z \left[1 + \left(\frac{z_0}{z} \right)^2 \right]. \quad (3)$$

W gives the radius of the beam at the coordinate z (i.e it is the distance in the x-y plane for which the intensity of the beam is $1/e^2$ the intensity at the origin of the plane):

$$W(z) = W_0 \sqrt{1 + \left(\frac{z}{z_0} \right)^2} \quad (4)$$

W_0 is the radius at $z=0$, and z_0 is the Rayleigh range defined as

$$z_0 = \frac{\pi W_0^2 n}{\lambda},$$

being λ the wavelength and n the refractive index of the medium in which the beam is propagating. The Beam Waist and the Radius of curvature at a particular point contain all the informations on the characteristics of the beam. Therefore by knowing these 2 parameters, we can determine the characteristics of a Gaussian beam after any optical element. For this we need to introduce the complex beam parameter $q(z)$:

$$q(z) = z + iz_0 \iff \frac{1}{q(z)} = \frac{1}{R(z)} - i \frac{\lambda}{n\pi W^2(z)}. \quad (5)$$

From the ray transfer matrix method we know that every optical element can be described by a matrix:

$$\begin{pmatrix} A & B \\ C & D \end{pmatrix}$$

It can be demonstrated that if q_{in} is the complex beam parameter of the gaussian beam before the optical element, after the optical element the complex beam parameter is given by the following equation:

$$q_{out} = \frac{Aq_{in} + B}{Cq_{in} + D} \quad (6)$$

Moreover if several optical elements are cascaded one after another, they can be described by a single matrix which is the product of the single matrices (the order of the multiplication of the matrices is from the last element to the first one). The reader who wants to know more about Gaussian beams and Matricial Optics, can find a more detailed explanation in any Optics book, such as [2]

1.2 Finding the optimal lenses configuration

Using the ray transfer matrix method introduced above, it has been implemented a Matlab routine that given an arbitrary number of lenses, calculates the optimal positions and focal lengths in order to have the maximum amount of light coupled from the optical fiber into the cavity. The fixed parameters in the simulation are the Mode field diameter of the optical fiber, the length of the cavity and the characteristics of the mirrors of the cavity. In particular the spherical mirrors ($R_{mirror} = 50\text{mm}$) and the length of the cavity ($L=94\text{mm}$) impose a condition on the beam that resonates inside the cavity: the Gaussian beam in correspondance of the mirror needs to have the same radius of curvature of the mirror. From this condition and using equation 3, one can calculate the waist of the beam inside the cavity that in our case is:

$$R\left(\frac{L}{2}\right) = \frac{L}{2} \left[1 + \left(\frac{2z_0}{L}\right)^2 \right] = R_{mirror} \rightarrow W_0^{target} = 63.4\mu\text{m} .$$

In order to couple the maximum amount of light into the cavity, we need that after the beam propagates through all the optics and enters the cavity, it has the waist in the middle of the cavity and it needs to match W_0^{target} . Keeping that in mind, the Matlab software works as follow: you select an arbitrary number of lenses (which are initially considered as thin lenses), and the parameters that you want to keep fixed (focal length and position of each lens). You insert values for the fixed parameters and consider all the other parameters as free. Then you build the

transfer matrix for each optical component (NB that also the propagation of the beam through air has to be considered, and therefore is represented by a matrix), and multiply them together in order to obtain the total transfer matrix of the system. We completely know the complex beam parameter in input of this matrix, since it is solely dependent on the characteristics of the optical fiber (MFD). The complex beam parameter in output of the system (q_{out}) is then calculated using equation 6, and it will be a function of the free parameters. About the target complex beam parameter (i.e the complex beam parameter that I expect in the centre of the cavity in order to have perfect coupling between optical fiber and cavity), we know by equation 5 that its real part has to be 0 since it is the reciprocal of the radius of curvature and for the symmetry of the cavity, the radius of curvature of a resonating beam is infinity at the waist's position. Therefore we can build an error function given by:

$$E = [Re(q_{out})]^2 + [z_0^{target} - Im(q_{out})]^2 . \quad (7)$$

Minimizing this function by means of the matlab routine `fminsearch`, we can find the values for the optimal values of the free parameters in order to have light resonating inside the cavity. Up to now, the Matlab software was modelling all the lenses as thin ones, which is not the case in reality. For this reason, once a thin lenses configuration is found, it is necessary to look for the availability of lenses that has the same (or close) focal length. After choosing the model of the lens, the Matlab routine reiterates the minimization process considering the lenses as real ones (therefore considering their thickness and radius of curvature of the surfaces). In this case, the radius of curvatures of the lenses and their thickness are kept as fixed parameters, and the parameters to be minimized are only their positions. This real configuration may not be as optimal as the ideal one: we need a way to theoretically calculate how much light is coupled into the cavity, also to check the correctness of the solution provided by the simulation. Since the Hermite-Gaussian modes form a base for the modes inside the cavity, the coupling can be calculated by decomposing the Gaussian beam entering the cavity into the Gaussian-Hermite modes supported by the cavity. The coupling will be given by the square modulus of the overlap integral between the normalized electric field of the incoming Gaussian beam and the complex conjugate of the normalized electric field of the TEM₀₀ mode supported by the cavity:

$$\eta = \left| \iint E_{00}^{beam} \tilde{E}_{00}^{cavity} dx dy \right|^2 \quad (8)$$

where E_{00} are given by equation 1 at the order $m=n=0$, apart from a normalization coefficient.

1.3 Behaviour of the system at cryogenic temperatures

Now that we know a configuration of lenses that couples light into the cavity, we want to know how the coupling will change when the system is cooled down at cryogenic temperatures. To do that we have to analyze the temperature dependence of the materials used in the simulation. For the metal structure that holds all the optical components it has been chosen Invar, because of its low coefficient of thermal expansion. For the lenses it has initially been chosen UV fused silica, because it also has a very low coefficient of thermal expansion, and it is well suited to work at cryogenic temperatures. In figure 1 is reported the linear thermal expansion of invar at different temperatures, as measured in [3]. In figure 2 is reported the linear thermal expansion of UV fused silica at different temperatures, as measured in [4] and in table 1 is reported the dependence of the index of refraction on the temperature for $\lambda = 1064nm$, as measured in [5].

T [K]	30	50	80	120	160	200	240	295
n []	1.44947	1.44950	1.44957	1.44970	1.44989	1.45012	1.45039	1.45082

Table 1: Refractive index as a function of temperature, for Fused Silica ($\lambda = 1064nm$).

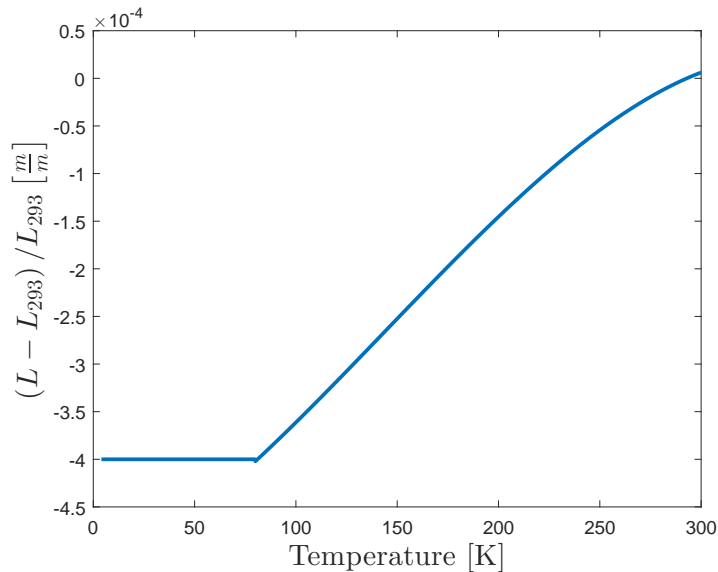


Figure 1: Linear thermal expansion for Invar as a function of temperature. L_{293} is the length at room temperature, and L is the length at the temperature considered. Note that this function is a fitting function of the data measured in [3].

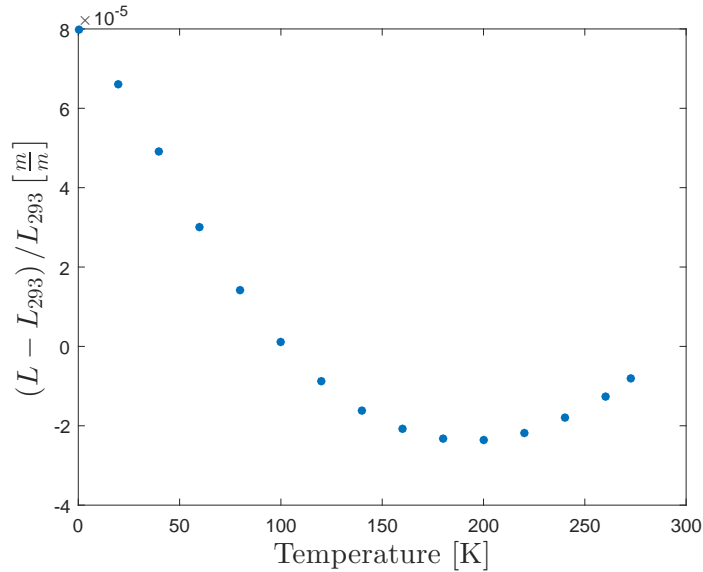


Figure 2: Linear thermal expansion for UV fused silica as a function of temperature. L_{293} is the length at room temperature, and L is the length at the temperature considered.

The thermal contraction/expansion of the materials causes a change in the position of the optical elements, and combined with the change in the refractive index causes also a change in the focal length of the lenses. To take these effects into account, a Matlab simulation has been implemented: once an optimal solution for the positions of the lenses is found using the previous simulation routine, the values are inserted in this other Matlab routine that taking into account of all the effects described, compute how much the coupling changes when going from room temperature to mK temperatures. Note that below 30 K we don't have data about the refractive index for fused silica, since it couldn't be found in literature. Nevertheless at that temperature the big changes in the properties of the material have already happened, and therefore it is possible to assume that the system doesn't change much from 30 K to mK temperatures.

1.4 Results of the simulations

Using the simulations previously described, it has been found a configuration of 2 lenses that theoretically couples 100% of the light from the optical fiber to the cavity. Note that this theoretical value of 100% is not realistic but just means good coupling, since the simulation didn't consider effects of aberration, absorptions and reflections of the lenses (which in the implementation of the setup will be

reduced by using aspherical lenses with anti-anti reflection coating) and considered the optical fiber, lenses and cavity to be perfectly centered along the z axis. Then the parameters of the 2 lenses were given in input to the software that calculates the change in coupling when going from room temperature to mK temperatures. In order to find the temperature-sensitive parameter that affects the coupling the most, the simulation has been run many times every time fixing a different parameter (so that it cannot change with the temperature) and calculating the final coupling at cryogenic temperature. By doing this it has been found out that the thermal expansion/contraction doesn't play an important role (distances and radiuses of curvature of the lenses doesn't change significantly to affect the coupling). What has been found to be the main contribution in the loss of coupling is the variation in the index of refraction of the first lens (the one closer to the tip of the optical fiber), that for UV fused silica is (normalized by the refractive index at room temperature):

$$\frac{n_{30} - n_{295}}{n_{295}} = -9.0 \times 10^{-4}$$

Using again the simulation, it has been noticed that the change in the refractive index doesn't play a big role if the first lens has a short focal length (roughly 4mm) and it is placed at a small distance from the optical fiber. However after a search we didn't find any manufacturer that produces such a short focal length lens made out of fused silica, therefore we considered different materials for the lenses. A good solution has been found in N-BK7 which has a lower variation in the index of refraction, as measured in [6]. The normalized change in the refractive index when going from room temperature to 60K is:

$$\frac{n_{60} - n_{295}}{n_{295}} = 8.6 \times 10^{-5}$$

which is roughly one order of magnitude lower than the one for fused silica at the same temperature range. The only drawback is the higher linear thermal expansion, compared to fused Silica. As measured in [7], the normalized linear thermal expansion from 300K to 30K is

$$\frac{L_{30} - L_{300}}{L_{300}} = -6.0 \times 10^{-4}$$

This could tilt the lens during the cool down, therefore particular attention should be paid in the design of the mountings for the lenses. In order to attenuate any aberration, we want the lenses to be aspherical: however we didn't find any manufacturer that produced aspherical lenses with relative short focal length in N-BK7. One of the common materials for aspherical lens with short focal length is dense Crown glass D-ZK3, which also happen to have similar thermal properties

to N-BK7, therefore this material has been selected for the lenses. The final configuration is made of 2 lenses: the first one has a focal length $f=4.5\text{mm}$ and it is positioned with its centre at $z_1=4.93\text{mm}$ from the end of the optical fiber, the second lens has a focal length $f=75\text{mm}$ and its center lies at $z_2=27.12\text{ mm}$ from the optical fiber. The distance fiber to first mirror is 50mm . When cooling down the system, the coupling at $T_f=40\text{ K}$ has been simulated to be 98% of the coupling at $T_i=300\text{K}$. In figure 3 is shown the beam diameter along the optical line for this configuration.

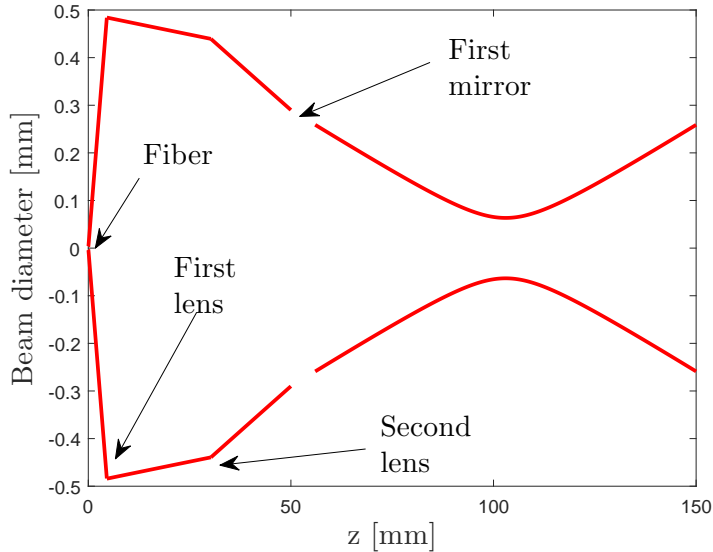


Figure 3: Beam diameter as a function of the position along the z axis for the final configuration of lenses: the coupling at 40K will be 98% of the coupling at 300K .

As a final remark, it is worth noticing that at room temperature, the precision with which the first lens is placed is critical to couple the light into the cavity, as shown in figure 4.

1.5 Experiment: testing the concept of the design

Up to now everything was simulated and in order to check if the axial symmetric design proposed is suitable for cryogenic applications, the next step is to test it experimentally. Given the complexity of the system, a lot of things can go wrong when cooling it down: therefore as a first experimental test we want to keep the system as simple as possible. Considering that the part that mostly affect the loss in coupling at cryogenic temperature is the first lens (and in particular its initial relative position with respect to the optical fiber as shown in figure 4),

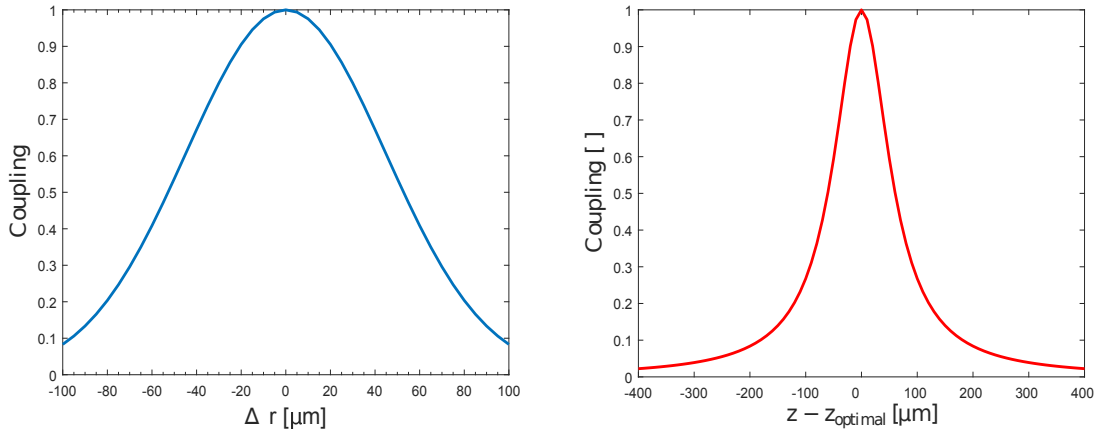


Figure 4: In figure is shown how the coupling is affected by a radial displacement of the lens on the xy plane (picture on the left), and by a displacement on the z axis with respect to the optimal position of the lens z_{optimal} (picture on the right).

initially only this part will be tested. This part has been manufactured by the fine mechanics department of Leiden University. It consist of a hollow invar cylinder with a fiber holder on one side, embedded in a differential screw that allows to move the position of the fiber along the axis of the cylinder with micrometric precision. Right after the fiber holder there is the lens support that allows to move the lens along the x-y plane (the plane perpendicular to the axis of the cylinder). At the other end of the cylinder there is a clamp mechanism that allows to connect the piece with other modules (in the future it will be the second lens and the cavity itself). The optical fiber used in the experiment is just PC (not angled), and it is kept in place inside the differential screw by a mechanism that clamp it on the end of the tip of the ferrule (in such a way that the thermal expansion of the ceramic ferrule doesn' t play any role in the experiment). Also the lens is clamped against the invar and kept in place by a spring loaded mechanism. No cryogenic glue has been used to fix the fiber or the lens, in order to avoid tilting of the optical components, as reported in [8]. For the purpose of the experiment, a part identical to the first one has been produced but without the differential screw, the fiber and the lens. On the side of this second part in which there should be the differential screw, a plane dielectric mirror has been glued using a very thin and uniform layer of STYCAST 2850FT (for cryogenic applications) as recommended in [8]. Then the 2 parts have been clamped together with screws. In figure 5 is shown a picture of the setup: on the right side of part A is visible the differential screw with the optical fiber plugged in. On the left side of part B is visible the mirror. In the two holes of part A can be inserted micrometric screw for the X-Y alignment of the lens (there are other 2 holes on the opposite sides of the visible ones, for a total of

1. FIBER TO CAVITY COUPLER FOR CRYOGENIC APPLICATIONS

4 micrometric screws in part A). It is also visible the temperature sensor Pt1000 used to monitor the temperature. The setup is mounted on a plate of a dilution refrigerator.

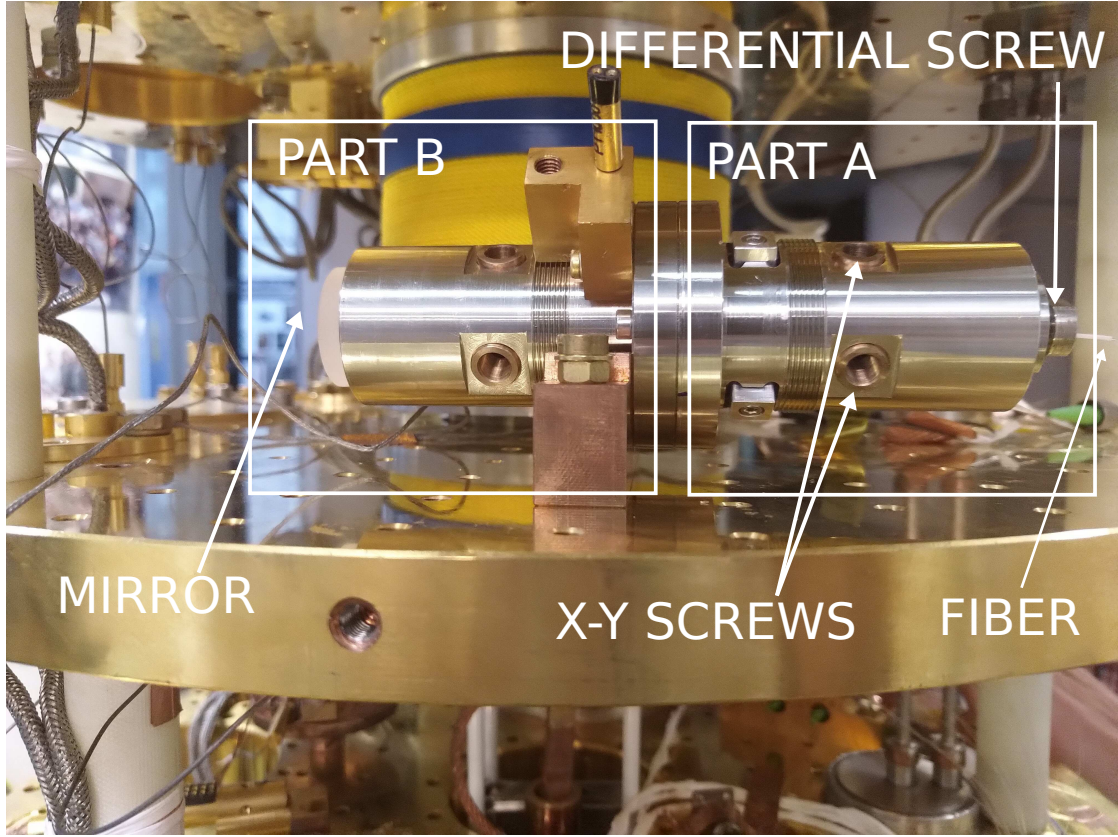


Figure 5: Fiber coupler used in the experiment with the name of the components. Notice that the X-Y screws are 4 (there are 2 more on the hidden side of part A).

The experiment consists in measuring the light that after being reflected by the mirror, is coupled back into the optical fiber, and monitor it at different temperatures. At room temperature the light coupled back in the optical fiber is $\simeq 90\%$ of the light sent with the laser. It is important to start with a very high value because that means we are close to the optimal configuration. In figure 6 is shown the schematic of the optical line used in the experiment: the laser light goes through a Faraday isolator (to prevent reflected light to go back into the laser), and then it is coupled into a SM fiber. This fiber is connected to port 1 of an in-fiber beam splitter that separate the light beam into 2: one goes to the fiber coupler device (port 3), and the other goes into a photodiode (port 4) in order to monitor the power of the laser over time. The light that goes into the fiber coupler is back reflected by the mirror, coupled again into the fiber and exiting through port 2,

1. FIBER TO CAVITY COUPLER FOR CRYOGENIC APPLICATIONS

after which is placed a photodiode that monitor the power over time. Finally the fiber coupler device is placed into a Cryostat: a dilution refrigerator, that allows to cool down the system at cryogenic temperatures in a slow and controlled way (starting from room temperature, it takes about 5 days).

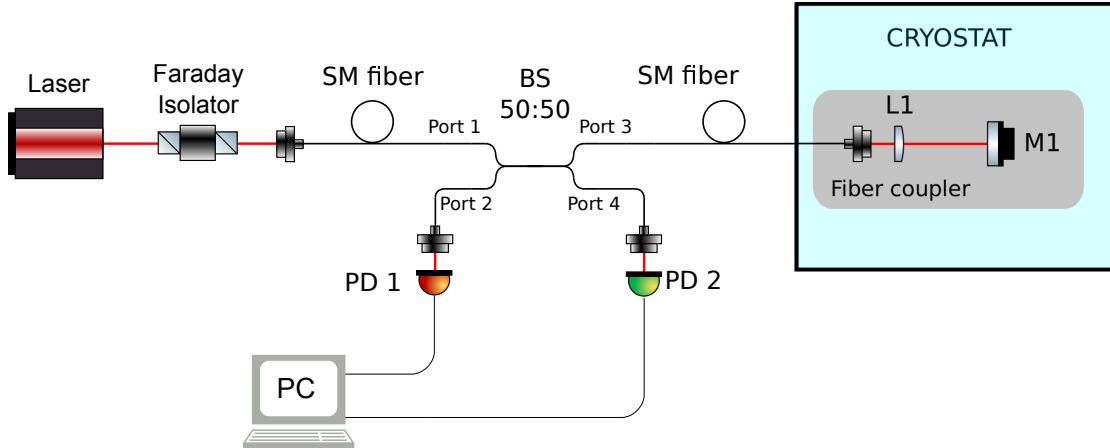


Figure 6: Optical scheme of the experiment

To monitor the temperature, 2 thermometers have been used: a Pt1000 attached directly on the fiber coupler structure (see part B in figure 5) which gives reliable measurements up to $\sim 20K$, and another custom-made resistive thermometer of Ruthenium Oxide, which is mounted on another plate in the same cryostat and it is suitable for a range of temperature from few K to mK. Notice that the cryostat has different cooling plates, stacked on top of each other: our experiment is mounted on the second-last of these plates, which reach as a lowest temperature 4K. The last plate of the cryostat reaches mK temperature, and it is where the other thermometer (Ruthenium oxide) is mounted. We are not interested in going to mK temperatures because the mechanical and optical properties of the material don't change anymore. We just mentioned that the 2 thermometers are mounted on different plates because as it is visible in figure 7, the readings of the 2 thermometers don't overlap in any range of temperature (they should at around 20 to 15 K). Indeed they are mounted on different plates, and it takes some time for the heat to propagate along different plates, leading to different temperatures between the plates.

In the same figure it is also visible that at the beginning of the experiment, the cryostat has been cooled to ~ 250 K, then heated up again and then the complete cooling down to 4 K started. This happened because of some technical problem with another experiment running in the same cryostat, but it provided us with useful information about our setup. Indeed We noticed that during this short cooling phase the coupling of the system decreased, but it went back to the initial

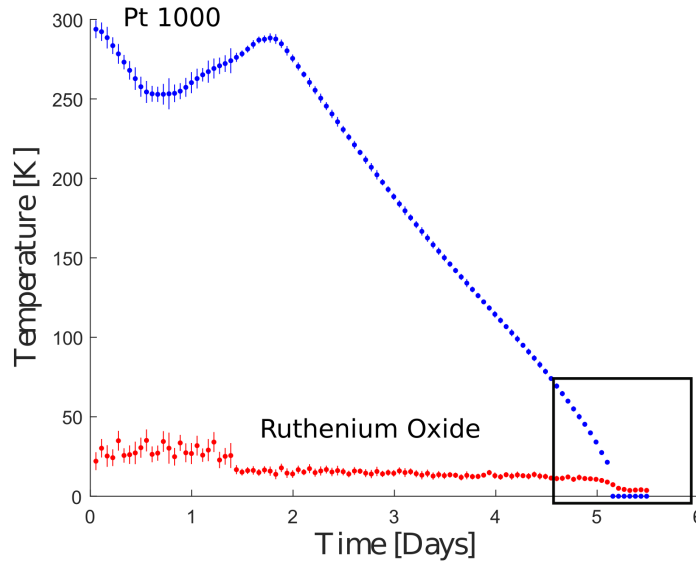


Figure 7: The plot shows the the temperature measured with the 2 thermometers as a function of time. In the highlighted region it is visible the point at which the Pt1000 stops working.

value once the system was brought back at room temperature. This means that nothing bad (i. e. irreversible processes) happened in our prototype, and it can be cooled down several time without the need of realigning the system every time. We will now quantitatively analyze the collected data shown in figure 8, in which we considered only the "real" cool down process, therefore neglecting the initial phase in which the system was cooled down and heated up again. Because of what said previously about the thermometers, the red line in the plot (placed at about 16 K) indicates the region over which the measured temperature is the real temperature of the system. This is not a big problem because not much happens below 16K for the purpose of our experiment.

The data have been filtered by means of a movable mean filter, in order to remove some noise. They show the back reflected light measured by photodetector (PD1 in the schematics of the optical line). The data have been normalized by the power of the laser (monitored separately by another photodiode as shown in the optical scheme in figure 6) in order to eliminate the effect of any change in the laser's power. The data have also been normalized by the measured back reflected light at room temperature, in such a way that at room temperature the measured intensity (power) is 1. Looking at the data it is immediately noticeable the presence of some oscillations: these are due to interference between the light promptly reflected by the mirror, and the light reflected by the tip of the optical

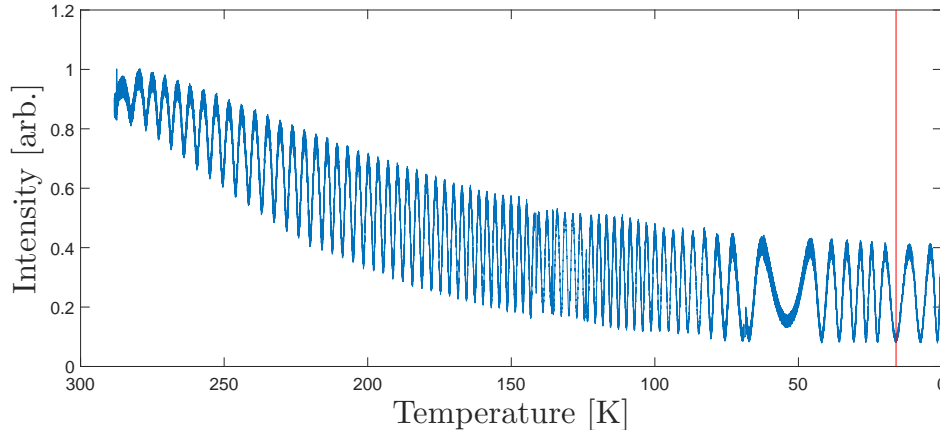


Figure 8: The blue signal is the back reflected intensity (power) as a function of temperature. It has been normalized in such a way that at room temperature its value is 1. The red line represents the point after which the temperature measured with the thermometer can not be trusted anymore.

fiber, which in this setup doesn't have any antireflection coating. Indeed when the temperature changes, the invar structure shrinks changing in this way the optical path of only the promptly reflected beam. Moreover we are sure that the stray reflection happens at the tip of the optical fiber because the only other element that could reflect some light is the lens, but the light back reflected by the lens is not mode matched with the optical fiber and therefore can not propagate inside it.

As an evidence that this effect is indeed interference, at some point we changed the frequency of the laser, and the effect of this process can be seen as a change in the phase of the oscillations in a zoomed in picture of the plot, shown in figure 9. At around 60K in figure 8 is also visible an inversion in the direction of changing of the phase of the oscillation: we think what is happening here is that at this temperature the coefficient of thermal expansion of invar becomes positive. In the plot of the linear thermal expansion of Invar (figure 1) this happens at around 80K (even though it is a minimal effect, and it is barely visible). The discrepancy between the 2 temperatures could be caused by a slight variation in the percentage of Nickel contained in the two alloys. Let's then move forward to the analysis of the data: in order to know what is the effective change in the coupling at different temperatures, we can not simply calculate the ratio between the backreflected intensities at the two temperatures, but we have to fit the data using the formula for total intensity of two interfering beams:

$$I_{tot} = I_1 + I_2 + 2\sqrt{I_1 I_2} \cos(\Delta\phi) , \quad (9)$$

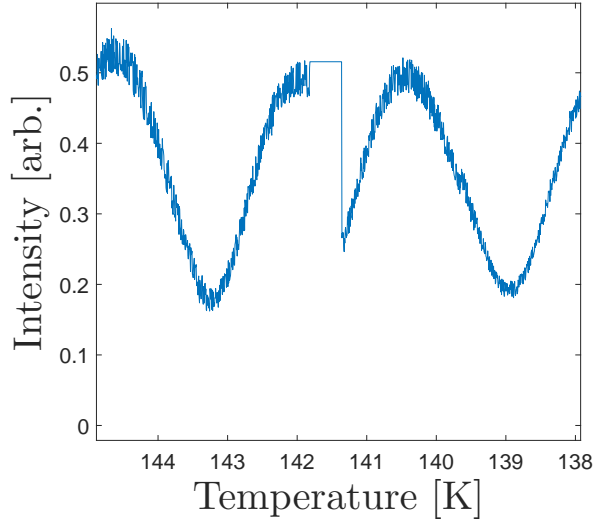


Figure 9: In figure is shown the change in the phase of the oscillations of the signal when we changed the frequency of the laser.

where I_1 and I_2 are the intensities of the 2 beams, and $\Delta\phi$ is the difference in the phase of the 2 beams. In the experiment the physical quantity measured is not the intensity but the power, which is the intensity integrated over the area of the photodetector hit by the laser beam. Since power and intensity differ just by a proportional coefficient, nothing changes in the analysis. During half a period of the oscillation the total intensity goes from a maximum (when $\Delta\phi = 0$) to a minimum ($\Delta\phi = \pi$). Equation 9 can therefore be rewritten as

$$\begin{cases} I_{max} = I_1 + I_2 + 2\sqrt{I_1 I_2} \\ I_{min} = I_1 + I_2 - 2\sqrt{I_1 I_2} \end{cases} \quad (10)$$

We measured the maxima and minima of the oscillations at room temperature ($T=288\text{K}$) and at 4K, and by inverting equation 10 we retrieved I_1 and I_2 that will be respectively the light reflected from the mirror, and the one reflected by the optical fiber. The change in I_1 tells us how much the coupling changes. The results are shown in table 2, in which the intensities are unitless because of the normalization explained previously.

Temperature	I_1 []	I_2 []
288 K	0.89 ± 0.01	0.016 ± 0.002
4 K	0.22 ± 0.02	0.025 ± 0.002

Table 2: Measured normalized intensities of the interfering light beams, at room temperature and at cryogenic temperature.

From these values we can calculate the coupling efficiency between room temperature (T=288K) and cryogenic temperature (T=4K), obtaining the following value:

$$\eta = \frac{I_1^{288K}}{I_1^{4K}} \simeq 25\%$$

which means that of the light coupled back into the fiber at room temperature, roughly 25% will still be coupled after the system is cooled down. Looking at I_2 , it can be noticed that its values increase at low temperatures. Calculating the correspondent reflectance using the formula

$$R = \frac{I_2}{I_1 + I_2},$$

we find that:

$$R_{288K} = (1.8 \pm 0.2) \%$$

$$R_{4K} = (10 \pm 1) \%$$

These values are not in agreement with the reflectance that we expect for the interface glass-air at the tip of the optical fiber, which is calculated using the Fresnel equations at normal incidence:

$$R_{interface} = \left| \frac{n_{glass} - n_{air}}{n_{glass} + n_{air}} \right|^2$$

and gives the following value:

$$R_{interface}^{288K} \simeq 3.4\%$$

$$R_{interface}^{30K} \simeq 3.3\%$$

where we used the index of refraction of Fused silica given in table 1. We computed the reflectance at 30K instead of 4K because we didn't find the index of refraction of fused silica at that temperature in literature, anyway this doesn't change in a significative way to explain the discrepancy with the effective reflectance measured. No explanation has been found for this discrepancy, but this is not a real problem because in this experiment we just wanted to test how the coupling of the fiber coupler changes going to cryogenic temperatures.

1.6 Conclusions and future developements

It has been measured that at 4K the coupling is $\eta \simeq 25\%$ of the value it has at 288K: this doesn't agree with the simulation (which predicted a much higher value around 98%), but is still a very good result. We have some ideas about the factors

that could have caused this decrease in the coupling: first of all in the simulation we didn't consider aberrations, and even though the collimating lens is aspherical in order to correct for this effect, it doesn't completely eliminate it. That said, the main contribution in the loss of coupling has been identified in the differential screw: while aligning the system at room temperature we noticed that this part (on which is also mounted the ferrule of the optical fiber) is not very stable and whilst it is supposed to move only in the z direction (along which the light beam propagates), it slightly moved also along the x-y direction. This is a crucial part of the setup, because as shown in figure 4, a displacement (or a tilt) of the optical fiber of few tens of μm in the x-y plane, drastically affects the coupling, and we think that this is what happened during the cool down.

The final setup for the fiber to cavity coupler that does the mode-matching between the light coming out of the optical fiber and optical mode supported by the cavity, will consist of the fiber coupler (the system composed by fiber and first lens), a second lens and the high finesse cavity. As previously said the simulations predicted that at cryogenic temperature the most critical part was the fiber coupler. Since the very first test on the component showed that at cryogenic temperature there is still a decent amount of coupling, we can build the final setup following this path. In the future developments there will be an improvement of the differential screw in the fiber coupler, allowing an even higher coupling coefficient. After that the other two modules (second lens holder and optical cavity) can be manufactured and connected to the first module. This setup will allow the Bouwmeester group to perform cavity optomechanics experiment in the quantum regime.

2 Pound-Drever-Hall laser frequency stabilization

The frequency of lasers fluctuates due to many factors, such as thermal expansion of the active medium and/or of the laser cavity. In optomechanical experiments it is mandatory to have a source of light with a high frequency stability, and a way to keep the frequency stable is the Pound-Drever-Hall technique, developed in 1983. The idea is simple: the laser's frequency is measured with a Fabry-Perot cavity, and the measurement is fed back to the laser to suppress frequency fluctuations. Generally implemented using free space optics, in our experimental setup this technique is implemented using optical fiber connections, and in-fiber optics. Maybe due to this reason, the error signal used to keep the frequency stable presents some instability like wiggles or a time dependent shift of its baseline level, as shown in figure 10.

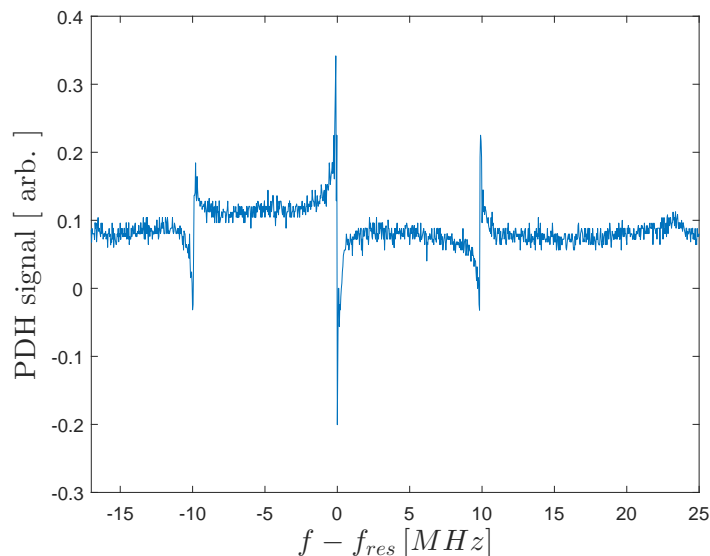


Figure 10: In figure is shown the PDH error signal of our setup. Here are visible the mentioned problems: the presence of wiggles in the signal, and a shift of the baseline level. Both of them fluctuates over time.

Because of this problem the frequency of the laser can not be kept stable for a sufficient amount of time to allow long measurements. In the first part of this chapter we will introduce the PDH frequency stabilization technique, and in the second part we will investigate and solve the abovementioned problems.

2.1 The general idea

The idea behind frequency stabilization techniques is to use a Fabry-Perot cavity to measure the frequency of the laser. A cavity acts as a filter: light can pass through a cavity only if the frequency is an integer multiple of the cavity's free spectral range $\Delta\nu_{FSR} = c/2L$ (L is the length of the cavity). The resonances (or transmission lines) are evenly spaced in frequency every free spectral range. If we operate near these resonances, such that some light is transmitted, then a small change in the frequency would produce a proportional change in the transmitted intensity. If we measured the transmitted intensity of the light, then we could feed this signal back to the laser in order to hold this intensity (and therefore the laser frequency) constant. This is how lasers were stabilized in frequency before the development of the PDH technique. It is straightforward to see that there are a few flaws in this technique, for example the system can not distinguish between fluctuations in frequency (that translates in fluctuations of the transmitted intensity) and fluctuations of the laser's intensity itself. A solution could be measuring the reflected intensity and holding that to zero: in this way frequency noise is decoupled by intensity noise. The problem with this solution is that the intensity of the reflected beam is symmetric about the resonance: if the frequency drifts out of resonance, we can't tell just by looking at the reflected intensity, whether the frequency increased or decreased. However the derivative of the reflected intensity is antisymmetric about resonance, therefore we can vary the frequency a little bit and see how the reflected beam responds. The frequency is varied sinusoidally over a small range, and the reflected intensity varies sinusoidally in phase with the variation in frequency. By comparing the variation in intensity with the frequency variation, we are able to tell which side of the resonance we are on. Once we measure the derivative of the reflected intensity with respect to the frequency, we can feed this signal back to the laser to hold it on resonance.

2.2 Quantitative explanation

2.2.1 Reflection of a monochromatic beam from a Fabry-Perot cavity

To describe the behavior of the reflected beam, we consider the electric field at a fixed point outside the cavity. The magnitude of the incident beam is:

$$E_{in} = E_o e^{i\omega t}$$

The reflected beam is made up of two contributions: the beam promptly reflected by the cavity, and the leakage beam which is the part of the standing wave inside the cavity that leaks back through the input mirror. In order to calculate this field, one can consider that the light inside the cavity bounces back and forth for

2. POUND-DREVER-HALL LASER FREQUENCY STABILIZATION

an infinite amount of time. At every bounce the amount of light that leaks out of the first mirror is calculated, and all these contributions are summed up: the summation gives the reflected electric field. The reflection coefficient is defined as the ratio between the reflected and incident electric field:

$$F(\omega) = \frac{E_{ref}}{E_{inc}} = \frac{r \left(\exp\left(i \frac{\omega}{\Delta\nu_{FSR}}\right) - 1 \right)}{1 - r^2 \exp\left(i \frac{\omega}{\Delta\nu_{FSR}}\right)} \quad (11)$$

where, r is the amplitude reflection coefficient of the mirror and $\Delta\nu_{FSR}$ is the free spectral range of the cavity. In figure 11 are shown the intensity and the square modulus and the phase of the reflection coefficient $F(\omega)$.

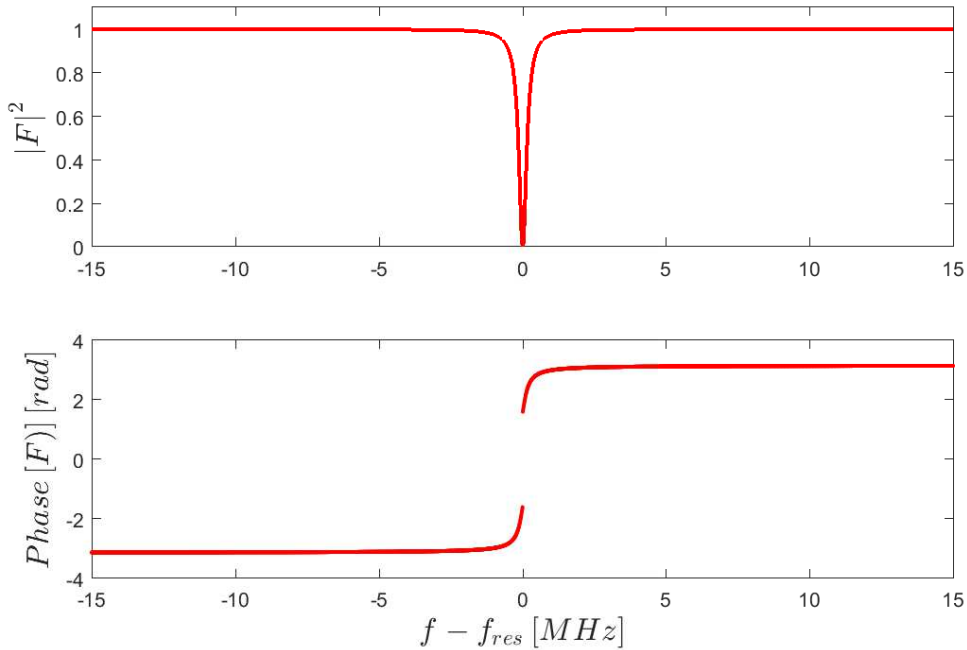


Figure 11: Phase and square modulus of the reflection coefficient of a Fabry-Perot cavity. It is visible a discontinuity in the phase for resonant frequencies.

From the plot of the phase of the reflection coefficient, it is immediate to understand that the phase of the light reflected from the cavity tells us which side of the resonance we are. The PDH technique provides us a way to indirectly measure the phase of the reflected electric field. As said previously, varying the frequency of the laser is enough to tell us which side of the resonance we are on: modulating the laser's frequency (or phase) will generate sidebands with a definite phase relation. Interfering these sidebands with the reflected beam, will create a beat pattern at

the modulation frequency and the phase of this beat pattern will tell us the phase of the reflected beam.

2.2.2 Beam modulation: sidebands

Varying the frequency of the beam produces the same results as varying its phase. The latter approach however is simpler. Phase modulation can be achieved by passing the beam through an EOM that is set to work as a phase modulator only (EOM in fact can work as a phase or amplitude modulator). If $E = E_0 e^{i\omega t}$ is the electric field entering the EOM, the electric field after the modulator is described by:

$$E_{inc} = E_0 e^{i(\omega t + \beta \sin(\Omega t))},$$

where Ω is the modulation angular frequency, and β is the modulation depth. We can expand this expression as a power series (a more formal way is to expand it using Bessel's functions, but the result is the same).

$$E_{inc} \simeq E_0 (1 + i\beta \sin(\Omega t)) e^{i\omega t} = E_0 \left(e^{i\omega t} + \frac{\beta}{2} e^{i(\omega+\Omega)t} - \frac{\beta}{2} e^{i(\omega-\Omega)t} \right). \quad (12)$$

Written in this way, it is easy to see that the modulated beam is made of three separate beams at different frequencies: a carrier at angular frequency ω and two sidebands at angular frequencies $\omega \pm \Omega$.

2.2.3 The error signal

The total electric field reflected by the cavity is given by the sum of the 3 beams at different frequencies, multiplied by the reflection coefficient at the frequency of the beams:

$$E_{ref} = E_0 \left[F(\omega) e^{i\omega t} + \frac{\beta}{2} F(\omega + \Omega) e^{i(\omega+\Omega)t} - \frac{\beta}{2} F(\omega - \Omega) e^{i(\omega-\Omega)t} \right]$$

The physical quantity we are interested in is the power of the reflected beam, since that is what the photodetector measures: $P_{ref} = |E_{ref}|^2$. Performing the calculations:

$$\begin{aligned} P_{ref} = & P_0 |F(\omega)|^2 + \frac{\beta^2}{4} P_0 \{ |F(\omega + \Omega)|^2 + |F(\omega - \Omega)|^2 \} \\ & + P_0 \beta \{ \text{Re} [\gamma(\omega, \Omega)] \cos(\Omega t) \\ & + \text{Im} [\gamma(\omega, \Omega)] \sin(\Omega t) \} + (2\Omega \text{terms}). \end{aligned} \quad (13)$$

where

$$\gamma(\omega, \Omega) = F(\omega) F^*(\omega + \Omega) - F^*(\omega) F(\omega - \Omega) .$$

2. POUND-DREVER-HALL LASER FREQUENCY STABILIZATION

In this expression the terms oscillating at frequency Ω are the result of the interference between the carrier and the sidebands, whilst the 2Ω terms are due to the interference between the sidebands. The 2Ω terms are not calculated explicitly since we are only interested in the Ω terms, for they sample the phase of the reflected carrier. The signal outputted from the photodiode is then demodulated using a mixer and a low pass filter. The mixer simply multiply the signal for an oscillating function at the same demodulation frequency Ω . Using some trigonometric formulas, it is straightforward to see that:

$$\sin(\Omega t) \sin(\Omega t) = \frac{1}{2} \{ \cos[(\Omega - \Omega)t] - \cos[(\Omega + \Omega)t] \} = \frac{1}{2} \{ 1 - \cos(2\Omega t) \}.$$

and

$$\sin(\Omega t) \cos(\Omega t) = \frac{1}{2} \{ \sin[(\Omega - \Omega)t] - \sin[(\Omega + \Omega)t] \} = -\frac{1}{2} \sin(2\Omega t).$$

From this identities we can see that mixing a sine and cosine signal instead of 2 sines, the DC term vanishes. The PDH error signal is given by the imaginary part of the $\gamma(\omega, \Omega)$ function, and therefore multiplying eq (13) by $\sin(\Omega t)$, and low pass filtering the result, we obtain the desired signal.

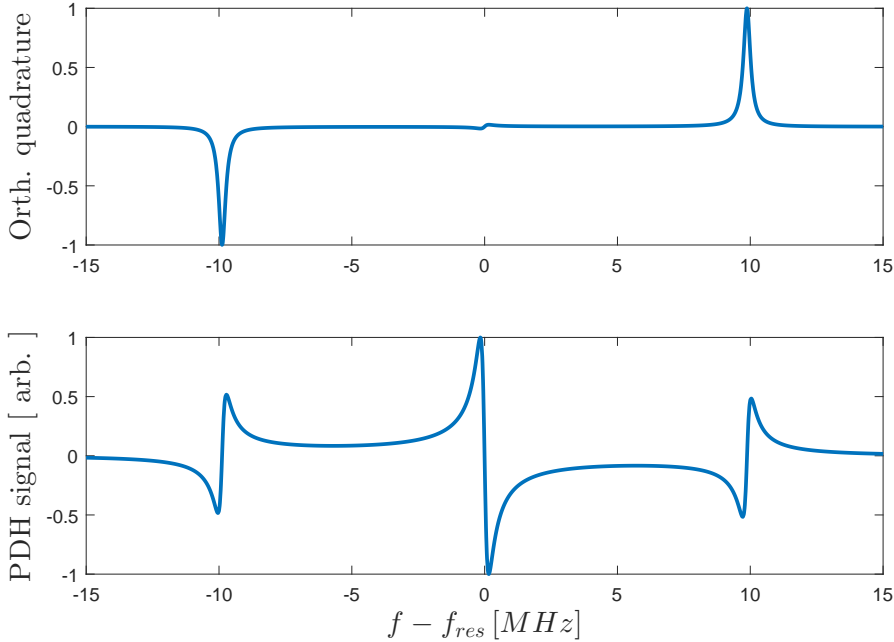


Figure 12: In figure are shown the PDH error signal as well as its orthogonal quadrature. These plots are made considering a cavity with Finesse 30000.

In practice the signal outputted from the photodiode is also phase shifted, because there are always unequal delays in the 2 signal paths (photodiode to mixer and oscillator to mixer). So in the end the signal is multiplied by $\sin(\Omega t + \phi)$. By changing this phase shift, we can go from a situation in which the error signal is purely made of the real part of the function $\gamma(\omega, \Omega)$ to a situation in which the error signal is purely made of the imaginary part of the same function. In figure 12 are shown both the PDH error signal (imaginary part of γ) and the orthogonal quadrature (real part of γ). Notice that the name orthogonal quadrature comes to the fact that we are demodulating with a phase shift of $\pi/2$. If the phase is chosen in between these 2 extrema values, then the error signal will have an odd looking shape, since it is made by a linear combination of the real and imaginary parts of $\gamma(\omega, \Omega)$.

To complete the frequency stabilization setup, the PDH signal is fed into a PID, that produces a control signal for the laser. The PID is set to work in the linear region of the error signal (the one at $f - f_{res} \simeq 0$ in figure 12): once the lock is established, if the frequency drifts the PID generates a signal that contains information on the amount and direction of drifting, and send it to the laser in order to correct for this drift.

2.3 The role of reflection

The experimental setup used to perform the measurements present a problem in the locking system for the lock is lost after a certain period of time, due to a shift in the level of the error signal that changed over time. Moreover the signal presented some wiggles. Therefore an extensive investigation has been carried out in order to understand the origin of the problem and to solve it. The main difference between this setup and the PDH setups described in literature ([9], [10], [11]) is that we are not just using free space optics, but also optical fibers and in-fiber optical components, as shown in figure 13. Therefore the first hypothesis was that there is some reflection happening at the interface between air and the optical fiber, that messes up with the Pound-Drever-Hall signal.

The first attempt to tackle the problem, consisted in considering the effect of a single reflection in the laser beam that is sent to the cavity. Referring to fig. 13 we considered reflection from the tip of the optical fiber in the path 2 of the circulator. The situation can be outlined as in fig. 14: calling r and t the reflection and transmission coefficient for the fiber to air interface, we can write the total electric field at the points indicated by 1, 2 and 3, considering that at the starting point (indicated by the origin of the arrows in the picture), the electric field is E_{in} .

$$E_1 = E_{in} t e^{ik\Delta x n_2}$$

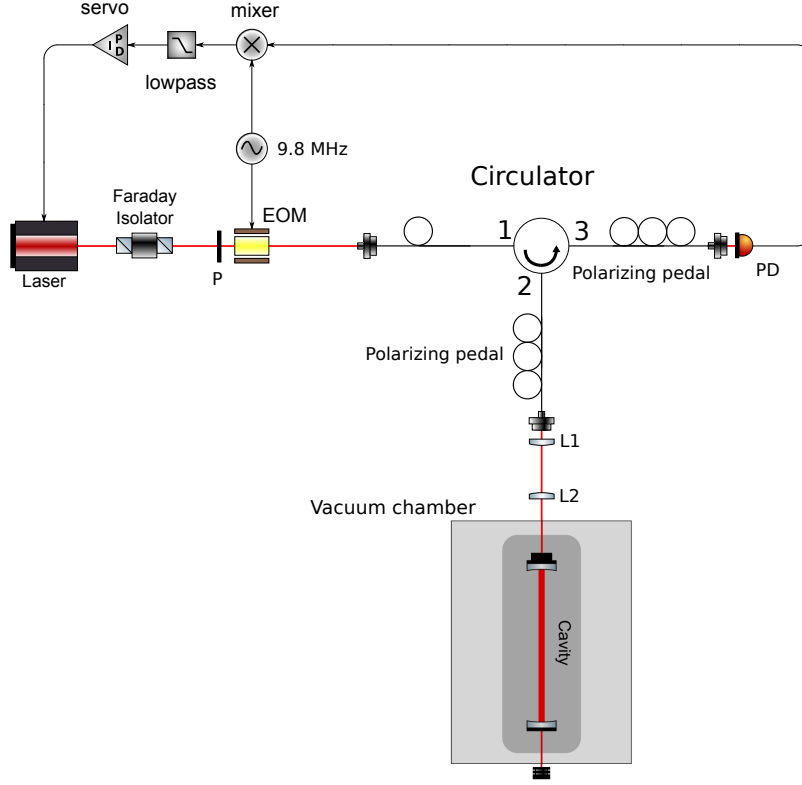


Figure 13: PDH setup used in the laboratory

$$E_2 = E_1 F(\omega) e^{2ikdn_1}$$

$$E_3 = E_2 t e^{ik\Delta xn_2} + E_{in} r e^{2ik\Delta xn_2}$$

where $F(\omega)$ is the reflection coefficient of the cavity given by eq. 11. The electric field E_3 is the sum of the electric field promptly reflected by the interface fiber-air and the one that is transmitted by the interface, reflected by the cavity and then transmitted again through the interface. The total electric field that goes to the photodetector is given by E_3 and it is:

$$E_{tot} = E_{in} e^{2ik\Delta xn_2} [t^2 e^{2ikdn_1} F(\omega) + r], \quad (14)$$

where the term outside the bracket is just a phase term dependent on the origin chosen and doesn't play any role since we are interested in the intensity (square modulus of the electric field).

At this point we can proceed with the same calculations done for the PDH error signal without reflections, with the only difference that now we won't consider just the reflectivity of the cavity, but the reflectivity of the system fiber + cavity, given by equation 15:

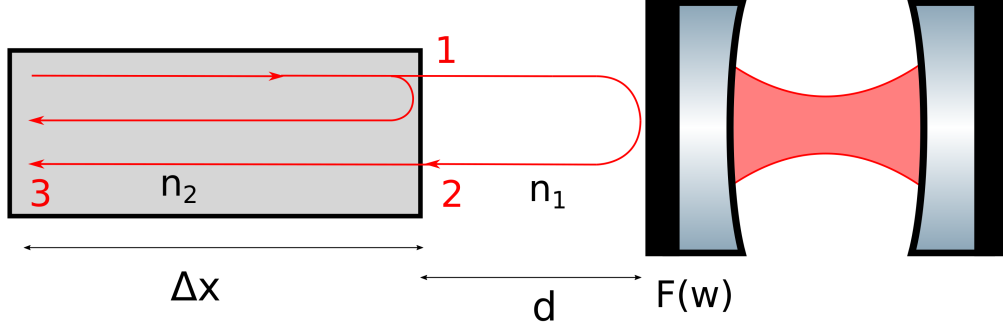


Figure 14: Reflection from the tip of the optical fiber in the PDH scheme

$$R(\omega) = t^2 e^{2ikdn_1} F(\omega) + r \quad (15)$$

The reflected power measured by the detector (neglecting the DC term that will be filtered out by the electronics after the photodetector) is :

$$P^{AC} = 2\sqrt{P_c P_s} \{ \text{Re}[\gamma(\omega)] \cos(\Omega t) + \text{Im}[\gamma(\omega)] \sin(\Omega t) \}, \quad (16)$$

where

$$\gamma(\omega) = R(\omega) R^*(\omega + \Omega) - R^*(\omega) R(\omega - \Omega).$$

The role of the mixer is to multiply the signal read by the photodetector by an oscillating signal at frequency Ω and phase shift it by ϕ . The resulting signal will be:

$$\begin{aligned} \epsilon = P^{AC} \cos(\Omega t + \phi) = \sqrt{P_c P_s} \{ & \text{Re}[\gamma(\omega)] (\cos(2\Omega t + \phi) + \cos(\phi)) \\ & + \text{Im}[\gamma(\omega)] (\sin(2\Omega t + \phi) - \sin(\phi)) \} \end{aligned} \quad (17)$$

Finally after the low pass filter, the remaining term is given by

$$\epsilon = \sqrt{P_c P_s} \{ \text{Re}[\gamma(\omega)] \cos(\phi) - \text{Im}[\gamma(\omega)] \sin(\phi) \} \quad (18)$$

Again the out signal is a linear combination of the 2 quadratures (real and imaginary part of the function $\gamma(\omega)$ in this case), and by properly selecting the phase we can isolate just the real part which corresponds to the PDH signal in presence of a reflection.

2.4 Simulations

From the calculations carried out in the previous section, we obtained an analytical (but very complicated) formula for the PDH error signal. In order to check if the

reflection could recreate the problem that we observed experimentally in the PDH signal, a simulation has been implemented using Matlab. In particular in this simulation we don't just simulate the error signal obtained in equation 18, but starting from an input electric field at the photodetector in the presence of a reflection, given by equation 14, we simulate the whole electronic chain in order to obtain an error signal that more realistically represents the one obtained in the real experimental setup. We also take into account the different index of refraction for the sidebands and for the carrier waves, since they have different frequencies. The dependence of the refractive index on the wavelength has been computed using Sellmeier equation:

$$n(\lambda) = \sqrt{1 + \sum_i \frac{B_i \lambda^2}{\lambda^2 - C_i}}, \quad (19)$$

where as B_i and C_i coefficient have been used the ones for fused silica. Another important thing is that while equation 11 assumes the ideal case in which there is no absorption in the mirrors of the cavity ($r^2 + t^2 = 1$), in reality there is a small absorption, and we are going to take it into account. In particular in case of absorption the reflectivity and transmittivity of the electric field are given by

$$|r|^2 + |t|^2 + A = 1$$

and for our mirrors $A = 75 \times 10^{-6}$, $|t|^2 = 25 \times 10^{-6}$ and $|r|^2 = 0.9999$. As an effect, the depth of the reflectivity is reduced and the dip of the reflected coefficient of equation 11 doesn't go all the way to zero at the resonance frequency of the cavity, but stops at a positive value.

With these considerations, equation 14 has been given in input to the Simulation. The software modulates the input electric field in order to create the 2 sidebands, and the power measured by the photodetector is calculated as the squared module of the sum of the electric fields of the carrier and of the sidebands. The resulting signal is multiplied by $\cos(\Omega t + \phi)$, where Ω is the modulation frequency, and ϕ is an adjustable phase term that allows to choose the quadrature of the PDH signal. Finally the signal is filtered using a low pass filter in the frequency space. The filter has been chosen with the same parameters of the electronic filter in the experimental apparatus, which is a low pass filter with a cut-off frequency at $200kHz$, and a slope of -20 db/dec. In order to retrieve the mathematical expression of this filter, we considered the transfer function of an passive RC low pass filter: writing down the transfer function of this circuit, we obtain:

$$H = \frac{Z_C}{Z_C + R} = \dots = \frac{1}{1 + j\omega\tau} \quad (20)$$

being the impedance of the capacitor $Z_C = 1/j\omega C$ and $\tau = RC$ the time constant. Considering that τ is also the reciprocal of the cut-off frequency, in the frequency

2. POUND-DREVER-HALL LASER FREQUENCY STABILIZATION

space the low pass filter is represented by the following mathematical expression:

$$H(f) = \frac{1}{1 + j\frac{f}{f_{3dB}}} , \quad (21)$$

where in our case $f_{3dB} = 200kHz$. In order to apply the filter, right after we multiplied the signal for $\cos(\Omega t + \phi)$, we Fourier-transformed it, multiplied it by $H(f)$ and finally antiTransformed it. The resulting signal is the PDH signal. In figure 15 is shown the resulting PDH error signal obtained considering an optical path difference OPL=3m, between the beam reflected from the cavity and the spurious reflection from the optical fiber tip. As reflection coefficient has been used the one for the interface glass-air given by Fresnel equation for normal incidence:

$$r = \frac{n_{glass} - n_{air}}{n_{glass} + n_{air}} \simeq 0.034$$

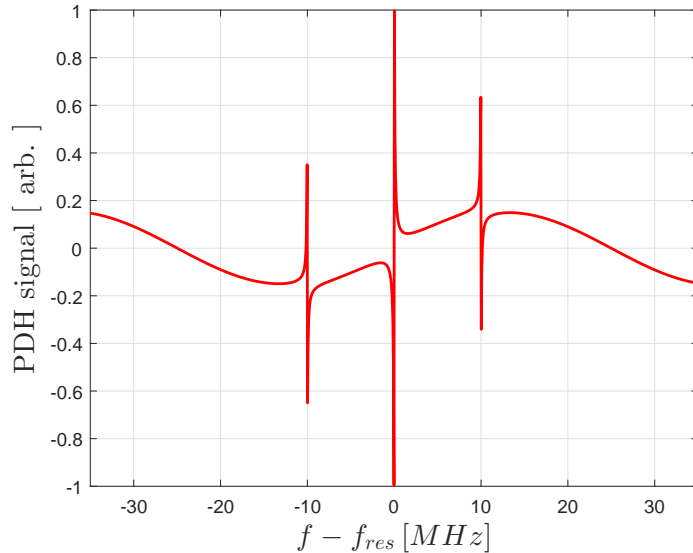


Figure 15: Simulated PDH signal in presence of a reflection. The appearance of the wiggles is visible.

The signal obtained from the simulation has the same characteristics of the signal we have in the real PDH setup. In the real experimental apparatus the wiggles are not stable in time: fluctuations in the temperature of the environment cause a change in the optical path difference (between the spurious reflection and the beam directly reflected from the mirror). As a result the oscillation visible in figure 15 shifts in frequency, making the central peak in the PDH signal shift up or down, depending on the point on which is situated on the wiggle. In the reality this effectively change the setpoint of the locking system, and the lock is lost.

2.5 Experimental verification

In order to check experimentally the model, we want to see if we are able to create the wiggles observed in the PDH error signal, by introducing a reflection in a controlled way. For this purpose another PDH setup has been implemented, using just free-space optics, as shown in figure 16. In this case instead of using the circulator, we are using a combination of a polarizing beam splitter and a quarter waveplate: after passing through the polarizing beam splitter and the quarter waveplate, the light will have circular polarization (let's say right circularly polarized). After the reflection from the mirror of the cavity the light will be circularly polarized but in the other direction (let's say left), and going back through the quarter waveplate it will have a linear polarization perpendicular to the one coming out of the PBS, and therefore will be sent to the photodetector that measures the reflected signal. Note that there is also another linear polarizer between the detector and the PBS to get rid of the light with the wrong polarization that hasn't been filtered out by the PBS (which is not ideal).

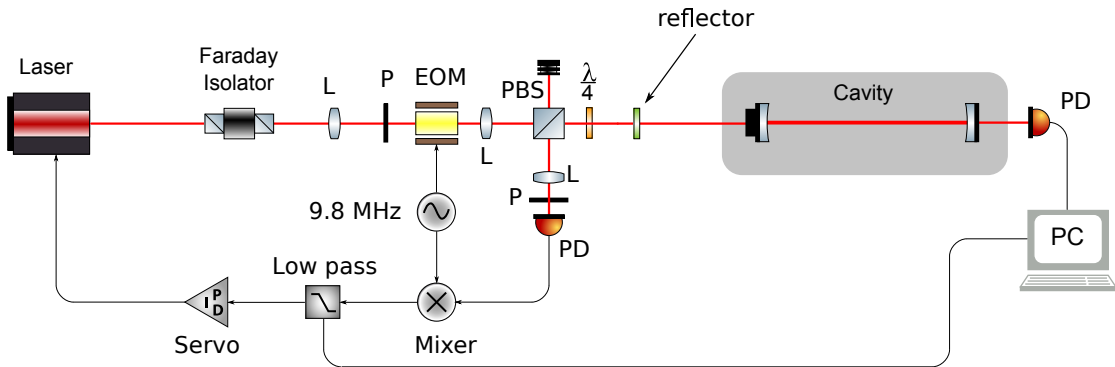


Figure 16: Setup used to investigate the role of reflections in PDH system, and to test the results of the simulations

By placing a reflective membrane in between the quarter waveplate and the cavity, we were able to observe the following: if the membrane was tilted so that the light reflected back from it didn't go back and impinged on the photodetector, we could observe a nice PDH signal. But carefully aligning the membrane so that the light back reflected from it impinged on the photodetector, we instantly noticed the appearance of the wiggles in the PDH error signal, monitored with an oscilloscope. By our theoretical model, and confirmed by calculating it in the simulation, the period of the wiggles is given by:

$$T_{frequency} = \frac{c}{2dn_1} \quad (22)$$

where d is the distance between the first mirror of the cavity and the reflector.

2. POUND-DREVER-HALL LASER FREQUENCY STABILIZATION

We placed the reflector at different positions, and we experimentally measured the period of the wiggles observing a very good agreement between the measured period and the one predicted by the model.

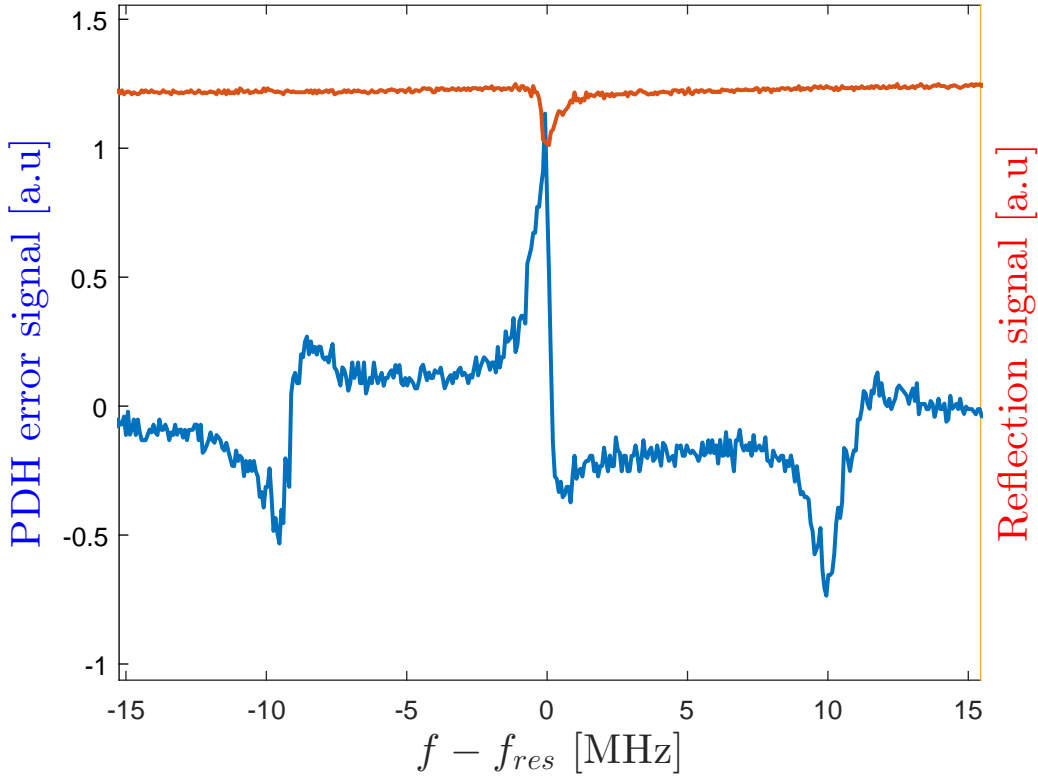


Figure 17: In blue the PDH error signal, in red the reflection signal. The data have been acquired with the reflector placed at $d=0.3$ m from the first mirror of the cavity. The presence of the wiggles can be seen looking at the reflection signal, and also looking at the shape of the PDH error signal: the peak corresponding to the carrier is not symmetric with respect to the x axis, a feature that emerges due to the wiggles.

In figure 17 is shown an example of the PDH error signal and reflection signal for this experiment. Notice that in this case the wiggles are not clearly visible in the PDH signal because it is not sharp enough (the cavity used for this experiment has a Finesse of about 2000, which lowers the sharpness of the signal). In order to measure the period of the wiggles we shifted the frequency of the laser far from the resonance frequency of the cavity, in order to observe just the baseline of the PDH signal without the peaks due to the carrier and sidebands. Note that in some situations the period of the wiggles cannot be directly seen in the oscilloscope, since the frequency range scanned by the laser is not broad enough to cover one period

of the wiggle. In this case on the oscilloscope the baseline level of the PDH error signal is shifted from 0, and in order to measure the period of the wiggles we manually changed the frequency of the laser (this allowed to cover a broader range of frequencies): in this way the baseline level of the PDH signal will shift, and the period of the wiggles is given by the frequency difference between 2 maxima of this baseline level.

Now that we are sure that the model works, we can consider again the original experimental setup sketched in figure 13. As mentioned before in this setup we observe the presence of wiggles and of a time dependent shift of the baseline level of the PDH error signal. Now we understood that this shift is just another wiggle in the signal, with a very long period. In particular we measured the periods of these 2 kind of wiggles, obtaining the following result:

$$T_1^{frequency} \simeq 45MHz \rightarrow d \simeq 3.3m$$

$$T_2^{frequency} \simeq 1.5GHz \rightarrow d \simeq 10cm$$

Both of these values are inconsistent with the hypothesis that the reflection happens at the interface between fiber optic and air. Checking the optical line, we notice that the optical circulator is placed at a distance of 2.5 m from the first mirror. Since light after the circulator travels through a 2m long optical fiber ($n \simeq 1.5$) and then through 0.5m of air, the total optical path length (OPL) is

$$OPL = 0.5m + 2m \times 1.5 = 3.5m$$

This suggests that the problem is in the circulator. To be sure of this, we changed the OPL by increasing the length of the optical fiber in the path 2 of the circulator (see figure 13), measured the corresponding period of the wiggles and compared this value with the Theoretical period predicted by the single reflection model. The results are summarized in table 3

OPL [m]	$T_{measured}$ [MHz]	$T_{theoretical}$ [MHz]
3.5	45	43
8	19	18.8
12	14	12.5

Table 3: In the table are shown the measured and predicted period of the wiggles, at different values of optical length after the port 2 of the optical circulator.

The measured and predicted values of the period are consistent with each other. The conclusion is that to cause this wiggle is not a reflection, but some stray light that goes directly from port 1 to port 3 of the optical circulator. We measured the power of this light, and it corresponds to an effective reflection coefficient for the electric field of

$$r_{eff} = 1.6 \times 10^{-3} .$$

2.6 Conclusions

During this section we showed how the simulations and experiments allowed us to understand the causes of the problem encountered in our PDH setup, which turned out to be interference either due to a non ideal optical circulator, or to some stray reflections in the optical line. In order to get rid of this problem, we inserted another polarizing pedals in path 2 and 3 of the circulator (see figure 13), and by carefully adjusting the polarization of the polarizing pedals, we formed an optical isolator that blocks the stray light that goes from path 1 to path 3.

As far as concern the wiggles with a period of 1.5 GHz, we checked in the optical table all the optics that could cause an optical path difference of 10cm between the main beam and the reflected one. We moved and tilted a little bit these optics (to make sure that possible reflected beams don' t go to the photodiode) in order to find the point in which the reflection was happening. The source has been identified in a double reflection inside the EOM: after carefully realigning it the problem was solved and now we are able to keep the laser locked for indefinite time (for sure days). This allows us to perform experiments that require a long time of data acquisition, such as the one described in the next section.

3 Decay of a thermomechanical squeezed state

To introduce the concept of thermomechanical squeezed state, let's have a look at the motion of a 1D mechanical oscillator:

$$x(t) = X(t) \sin(\Omega_m t) + Y(t) \cos(\Omega_m t) .$$

$X(t)$ and $Y(t)$ are called quadratures, and are the time dependent coefficients of the sine and cosine components of the motion of the oscillator. In normal conditions X and Y have the same variance at fixed temperature. A thermomechanical squeezed state is defined to be the state of a mechanical oscillator in which the variances of the 2 quadratures are not equal: in particular there is a squeezed quadrature (in which the value of the variance is reduced) and an amplified quadrature (in which the variance is increased). The reduction and amplification in the variances is with respect to the variance that the mechanical oscillator normally has at the same temperature. This thermomechanical squeezing has already been achieved in the Bouwmeester group [12] by parametric modulation of the spring constant. In this chapter we will explore what happens when this parametric modulation is turned off: in particular we want to find out how the squeezed state goes back to the non-squeezed one, and how much time it takes for this process to happen. This study is performed in the classical regime, nevertheless it is useful because it can be trivially extended to the quantum regime once the cryogenic optical cavity will be completed. Moreover studying this process will help us answering the question whether it is possible to swap a squeezed thermomechanical state between two different mechanical modes.

3.1 Mathematical description of squeezing

In order to create a squeezed state, it is necessary to parametrically modulate the spring constant. One way to do that is by using the radiation pressure force. Let's consider one mechanical mode of the membrane with angular frequency Ω_m . For this particular mode, the equation of motion can be written as

$$\ddot{x} + \frac{\Omega_m}{Q} \dot{x} + \Omega_m^2 x = f_{th}(t) , \quad (23)$$

where Q is the quality factor of the membrane and f_{th} is the thermal force per unit mass that is driving the oscillator. Assuming that $Q \gg 1$, the solution of the equation of motion can be written as:

$$x(t) = X(t) \sin(\Omega_m t) + Y(t) \cos(\Omega_m t) . \quad (24)$$

Here $X(t)$ and $Y(t)$ are the two quadratures, and are slowly varying compared to the mechanical (angular) frequency Ω_m ($\dot{X}, \dot{Y} \ll \Omega_m$). Now we add a parametric

3. DECAY OF A THERMOMECHANICAL SQUEEZED STATE

modulation of the spring constant in equation 23 and see how this affects the two quadratures in the solution of the equation. In order to squeeze one of the quadratures, the modulation of the spring constant has to be done at twice the mechanical frequency of the mechanical mode Ω_m we are considering, as it will be clear at the end of the demonstration. The equation of motion for this case becomes:

$$\ddot{x} + \frac{\Omega_m}{Q}\dot{x} + \Omega_m^2 [1 - \beta \sin(2\Omega_m t + \phi)] x = F_{th}(t) . \quad (25)$$

Here β is the spring constant modulation depth, and ϕ is just a phase term. As pointed out in [13], we can write the driving thermal force in a similar way of equation 24, since the resonator will respond to this force only in the proximity of its resonance frequency Ω_m :

$$F_{th}(t) = F_s(t) \sin(\Omega_m t) + F_c(t) \cos(\Omega_m t) , \quad (26)$$

also here the sine and cosine components (F_s, F_c) are slowly varying. By substituting equations 24 and 26 into equation 25, performing some calculations and by neglecting $2\Omega_m$ and $3\Omega_m$ terms, we can decouple the equation for the X quadrature from the equation for the Y quadrature, obtaining (for $\phi=0$):

$$\begin{cases} \dot{X} + \frac{\Omega_m}{2Q} \left(1 + \frac{\beta Q}{2}\right) X = \frac{F_c}{2\Omega_m} \\ \dot{Y} + \frac{\Omega_m}{2Q} \left(1 - \frac{\beta Q}{2}\right) Y = -\frac{F_s}{2\Omega_m} \end{cases} \quad (27)$$

We can see that this set of equation is Quadrature sensitive: the effective inverse Q factors for the X and Y quadratures are different from the one in the unpumped case:

$$\begin{aligned} X \text{ quadrature} : \quad \frac{1}{Q} &\rightarrow \frac{1}{Q} + \frac{\beta}{2} \\ Y \text{ quadrature} : \quad \frac{1}{Q} &\rightarrow \frac{1}{Q} - \frac{\beta}{2} \end{aligned}$$

From this it is straightforward that the response to a sine force f_s is amplified, being the effective Q factor of the Y quadrature higher. Whereas the response to a cosine force f_c is deamplified (X quadrature has a Q factor lower than the unpumped case).

Notice also that when the modulation depth β is equal to $\beta_{cr} = \frac{2}{Q}$, the effective Q factor becomes zero and the amplified quadrature Y becomes unstable. This phenomenon is called parametric instability, and it manifests for $\beta \geq \beta_{cr}$. It is useful to introduce a normalized gain parameter g , defined as:

$$g = \frac{\beta}{\beta_{cr}} = \frac{\beta Q}{2} , \quad (28)$$

3. DECAY OF A THERMOMECHANICAL SQUEEZED STATE

in such a way that $g=1$ leads to the parametric instability of the amplified quadrature. In order to solve the set of equations 27, we will go into the frequency domain. The power spectral density for the thermal forces f_s and f_c is given by [13] :

$$S_{f_s} = S_{f_c} = \frac{2k_B T_{eff} \Omega_m^3}{kQ}, \quad (29)$$

being k the spring constant of the mechanical oscillator. T_{eff} is the effective temperature, which takes into account the optical damping (see the next sections). Therefore in the frequency domain we have:

$$\begin{cases} \left| i\omega X[\omega] + \frac{\Omega_m}{2Q} \left(1 + \frac{\beta Q}{2}\right) X[\omega] \right|^2 = \frac{2k_B T_{eff} \Omega_m^3}{kQ} \\ \left| i\omega Y[\omega] + \frac{\Omega_m}{2Q} \left(1 - \frac{\beta Q}{2}\right) Y[\omega] \right|^2 = \frac{2k_B T_{eff} \Omega_m^3}{kQ} \end{cases} \quad (30)$$

and rearranging the terms, we obtain the Lorentzian power spectral densities for the two quadratures:

$$\begin{cases} S_{XX}(\omega) = \frac{k_B T_{eff} \Omega_m}{2kQ} \frac{1}{\omega^2 + \Omega_m^2 \frac{(1+g)^2}{4Q^2}} \\ S_{YY}(\omega) = \frac{k_B T_{eff} \Omega_m}{2kQ} \frac{1}{\omega^2 + \Omega_m^2 \frac{(1-g)^2}{4Q^2}} \end{cases} \quad (31)$$

In order to calculate the variances of the X and Y quadrature, we use the relation

$$\langle X^2 \rangle = \frac{1}{2\pi} \int_{-\infty}^{\infty} S_{XX}(\omega) d\omega,$$

obtaining:

$$\begin{cases} \langle X^2 \rangle = \frac{k_B T_{eff}}{2k} \frac{1}{1+g} \\ \langle Y^2 \rangle = \frac{k_B T_{eff}}{2k} \frac{1}{1-g} \end{cases} \quad (32)$$

It is straightfward to see that the variances in the two quadratures are scaled by a factor $1/(1+g)$ and $1/(1-g)$ with respect to the unpumped case, obtained by setting $g=0$. In this case equation 32 reduce to the classical equipartition result, for the variances of the 2 quadratures are equal. If one measures the X and Y quadrature in the unpumped case, what he will observe is a circle in the quadrature space (plotting the Y quadrature as a function of the X quadrature). This circle corresponds to a bidimensional gaussian distribution, with equal variances along the X and Y quadratures, as predicted by equation 32 for $g=0$.

On the other side if we apply the parametric modulation of the spring constant, one observes that the circle in the quadrature space becomes an ellipse that correspond

to a bidimensional Gaussian distribution having different variances along the X and Y quadratures, as shown in figure.

When we approach the instability point ($g \rightarrow 1$), the maximum achievable squeezing of the X quadrature is a factor 2, or equivalently 3dB. This is known as the 3dB limit, and cannot be surpassed in this simple scheme for the generation of a squeezed state unless applying some clever technique that forbid the amplified quadrature Y to diverge. As a final remark we notice that the set of equations 32 is valid only in the case $g < 1$. For $g > 1$ the resonator is driven in the Y quadrature, and this causes the thermal distribution to shift from the origin in the quadratures space.

Up to now we showed how parametrically modulating the spring constant of the mechanical resonator, it is possible to generate a thermomechanical squeezed state. We didn't say anything about how to generate this modulation of the spring constant. One way to do it (and the way we will use) is to exploit the radiation pressure force of light. In the next paragraphs we will show the characteristics of the mechanical resonator we are using, and the main optomechanical effects that allow us to achieve squeezing.

3.2 The Membrane

The mechanical oscillator we are using is a Silicon Nitride membrane, which dimensions of a $3\text{mm} \times 3\text{mm} \times 25\text{nm}$. Due to the geometry of the membrane (it is a square with a thickness that approaches to zero), the frequencies of the transversal vibrational modes can be expressed by:

$$\Omega_m(i, j) = \Omega_m(1, 1) \sqrt{\frac{i^2 + j^2}{2}} \quad (33)$$

where $\Omega_m(1, 1)$ is the fundamental frequency and i and j are integers number that denote the index of the mode: in particular $i+1$ and $j+1$ are the number of nodes of the oscillations along the x and y axis (in a reference frame in which the 2 sides of the membrane corresponds to the x and y axis). From this equation it appears that for every mechanical mode Ω_m , there is a higher order mode with double frequency $2\Omega_m$. If we want to modulate the spring constant at twice the mechanical frequency, we are going to excite the modes whose frequency is a multiple of $2\Omega_m$. In the reality this doesn't happen because the membrane presents some anharmonicity, and the higher order modes deviate slightly from the theoretical values given by 33. The membrane is manufactured at University of California Santa Barbara, by other members of the same research group, and it is special because it has an embedded phononic crystal obtained by pinching some holes with specific size and position along all the surface of the membrane, leaving just

3. DECAY OF A THERMOMECHANICAL SQUEEZED STATE

a flat spot in the centre which is where the laser will shine. In figure 18 is shown an image of the membrane in which is visible the phononic crystal.

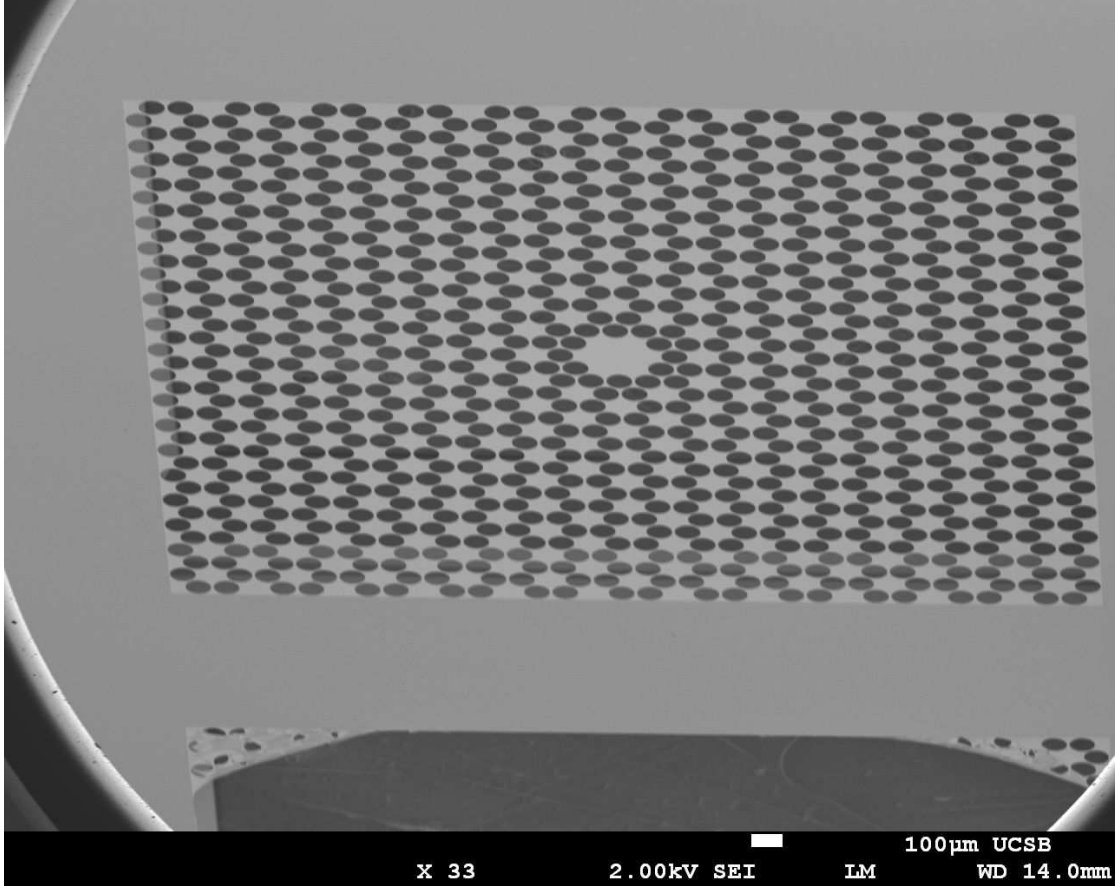


Figure 18: Electron microscope image of the membrane used in the experiment. It is visible the phononic crystal as a pattern of holes. The central area which is non-patterned, is the point on which will shine the waist of the laser beam inside the cavity.

This phononic crystal allows to obtain higher Q values for the different modes of the membrane. In this experiment we want to squeeze one quadrature of the (3,3) mode whose frequency is $\Omega_m(3,3) = 217kHz$. Another important parameter is the effective mass of the mode, which is equivalent to the mass that the mode would have if the membrane was an infinitesimal point. In order to calculate it let's define a 3D reference frame with the x and y axes aligned along the sides of the membrane, and with the z axis perpendicular to the membrane. The effective mass can be obtained by comparing the potential energy of a point like system that is oscillating along the z direction with maximum amplitude z_{max} , and the potential energy of the membrane when a stationary wave is present:

$$\frac{\Omega_m^2}{2} \int_{\Sigma} \rho(\vec{x}) z^2(\vec{x}) d\vec{x} = \frac{m_{eff} \Omega_m^2 z_{max}^2}{2} \quad (34)$$

where the integral is performed over the surface of the membrane, ρ is the density of the membrane and z is the displacement of the membrane due to the standing wave, as a function of the position along the x and y axes. By performing this calculation in COMSOL multiphysics, we obtain that for the (3,3) mode the effective mass is $m_{eff} = 73 \text{ pg}$.

3.3 Basics of the Optomechanical interaction

In this section we will introduce the basic concepts that describe the interaction between light and a mechanical resonator (inside a cavity). We are not going to go too much into details but the reader who wants to know more about it can use [1] and [14] as a reference.

3.3.1 Mechanical resonators

The mechanical resonator is an harmonic oscillator which is viscously damped and driven by a thermal force. The equation of motion is given by equation 23, but we are going to rewrite it expliciting the damping rate Γ_m :

$$m_{eff} \frac{d^2 x(t)}{dt^2} + m_{eff} \Gamma_m \frac{dx(t)}{dt} + m_{eff} \Omega_m^2 x(t) = F_{th}(t) \quad (35)$$

here F_{th} is given by the thermal Langevin force. $\Gamma_m = \Omega_m / Q_m$, where Q_m is the quality factor of the mode considered: having a higher Q_m means a lower coupling to the environment, which allows to the oscillator to be cooled at lower temperatures, as we will see in the following.

By defining the Fourier transform as $x(\omega) = \int_{-\infty}^{\infty} x(t) e^{i\omega t} dt$, and the susceptibility $\chi[\omega] = x[\omega] / F_{th}[\omega]$, we can solve equation 35 in the frequency domain:

$$\chi[\omega] = [m_{eff} (\Omega_m^2 - \omega^2) - im_{eff} \Gamma_m \omega]^{-1} . \quad (36)$$

In case Γ_m is small, the above equation can be approximated by a Lorentzian:

$$\chi[\omega] = (m_{eff} \Omega_m [2(\Omega_m - \omega) - i\Gamma_m])^{-1} .$$

Using the Fluctuation-Dissipation theorem, we can write the power spectral density of the mechanical oscillator:

$$S_{xx}[\omega] = 2 \frac{k_B T}{\omega} \text{Im}(\chi[\omega]) . \quad (37)$$

By substituting the imaginary part of the mechanical susceptibility (equation 36) into equation 37, we obtain

$$S_{xx}[\omega] = \frac{k_B T}{m_{eff} \Omega_m^2} \frac{\Gamma_m/2}{(\Omega_m - \omega)^2 + \Gamma_m^2/4} \quad (38)$$

which has a Lorentzian shape centered at Ω_m and a linewidth Γ_m . Using the Wiener-Kinchin theorem we can relate the Power spectrum to the variance of the mechanical displacement:

$$\langle x^2 \rangle = \int_{-\infty}^{\infty} S_{xx} \frac{d\omega}{2\pi} = \frac{k_B T}{m_{eff} \Omega_m^2} . \quad (39)$$

3.3.2 Light inside the cavity

One approach for describing the optical field inside a cavity is to describe the dynamics of the circulating intensity inside the cavity. To this purpose we can describe the field inside the cavity in terms of a complex mode amplitude $\alpha(t)$ such that $|\alpha(t)|^2$ is the photon number, or the stored energy:

$$\frac{d\alpha(t)}{dt} = -\frac{\kappa}{2}\alpha(t) - i\omega_{cav}\alpha(t) + \sqrt{\kappa_{ex}}\sigma_{in}(t) \quad (40)$$

where κ is the optical decay rate, ω_{cav} is the cavity frequency, κ_{ex} is the external optical coupling rate and σ_{in} is the input power. This classical equation has been derived by averaging its quantum version (see [1] for more details). A convenient way to solve equation 40 is to choose a coordinate frame rotating with the laser frequency ω_L , by defining:

$$\begin{aligned} \alpha(t) &= a(t) e^{-i\omega_L t} \\ \sigma_{in}(t) &= s_{in}(t) e^{-i\omega_L t} \end{aligned}$$

This yield to:

$$\frac{da(t)}{dt} = \left(i\Delta - \frac{\kappa}{2} \right) a(t) + \sqrt{\kappa_{ex}} s_{in}(t) , \quad (41)$$

where it has been introduced the laser detuning $\Delta = \omega_L - \omega_{cav}$. We are interested in a steady state solution of equation 41, which can be obtained by setting a constant input mode amplitude $s_{in}(t) = s_{in}$ and $da(t)/dt = 0$. This results in the mean mode amplitude

$$\bar{a} = \frac{\sqrt{\kappa_{ex} s_{in}}}{-i\Delta + \kappa/2} \quad (42)$$

3.3.3 Coupling of light with the mechanical oscillator

Now that we have provided a separate description of the mechanical oscillator and of the light field inside the cavity, we are going to see how the interaction between the two modifies their response. The following description is done for the case of

3. DECAY OF A THERMOMECHANICAL SQUEEZED STATE

a mechanical resonator as one mirror of the cavity, but it holds also for membrane in the middle systems, like the one we are using. The coupling of the mechanical motion to the cavity mode, modulates the cavity resonance frequency:

$$\omega_{cav}(x) = \omega_{cav} + x \frac{\partial \omega_{cav}}{\partial x} . \quad (43)$$

This linear approximation is valid only in case of small mechanical motion. We define the optical frequency displacement $G = -\partial \omega_{cav} / \partial x$. The displacement of the membrane causes the cavity resonance frequency to change as $Gx(t)$. Equation 41 therefore becomes

$$\frac{da(t)}{dt} = \left(i(\Delta + Gx(t)) - \frac{\kappa}{2} \right) a(t) + \sqrt{\kappa_{ex}} s_{in}(t) \quad (44)$$

We can now write the radiation force arising from the momentum transferred by the photons to the membrane. The momentum transferred by a single photon is $2\hbar k$, and the cavity round trip is $c/2L$. Being the total number of circulating photons $\bar{n}_{cav} = |a(t)|^2$, the radiation pressure force reads:

$$F_{rad} = \frac{\Delta p}{\Delta t} = |a(t)|^2 \frac{c}{2L} 2\hbar k = \hbar G |a(t)|^2 , \quad (45)$$

where $G = \omega_{cav}/L$. This allow us to write the modified equation of motion for the mechanical resonator, which now will be driven not only by the thermal force, but also by the radiation pressure force:

$$m_{eff} \frac{d^2 x(t)}{dt^2} + m_{eff} \Gamma_m \frac{dx(t)}{dt} + m_{eff} \Omega_m^2 x(t) = F_{th} + \hbar G |a|^2(t) . \quad (46)$$

Equations 44 and 46 are coupled non linear equations that describe the optomechanical interaction. In general they are difficult to solve, but we can find analytic solutions by making some assumptions: in the following we will assume that the motion of the mechanical oscillator is small, and that can be treated as a small perturbation around a mean displacement: $x(t) = \bar{x} + \delta x(t)$, and similarly for the cavity field: $a(t) = \bar{a} + \delta a(t)$.

The steady state solutions for equations 44 and 46 are:

$$\bar{a} = \frac{\sqrt{\kappa_{ex}}}{i(\Delta + G\bar{x}) - \frac{\kappa}{2}} s_{in} \quad (47)$$

$$\bar{x} = \frac{\hbar G}{m_{eff} \Omega_m^2} |\bar{a}|^2 . \quad (48)$$

3. DECAY OF A THERMOMECHANICAL SQUEEZED STATE

Using the perturbation assumption, and substituting equations 47 and 48 into 44 and 46, we obtain (after neglecting second order terms):

$$\frac{d\delta a(t)}{dt} = \left[-\frac{\kappa}{2} + i\Delta + iG\bar{x} \right] \delta a(t) + iG\bar{a}\delta x(t) \quad (49)$$

Using the same approach as for the uncoupled equations, we are going to solve it in the frequency domain, therefore by taking the Fourier transform, we obtain:

$$\delta a[\omega] = \frac{iG\bar{a}\delta x[\omega]}{\frac{\kappa}{2} - i(\Delta + G\bar{x} + \omega)} \quad (50)$$

Now we can calculate the radiation pressure force:

$$\begin{aligned} \delta F_{rad}(\omega) &= \hbar(\delta a(\omega) + \delta a^*(\omega)) \\ &= -\hbar G^2 \bar{a}^2 \left(\frac{\Delta + G\bar{x} + \omega}{\frac{\kappa^2}{4} + (\Delta + G\bar{x} + \omega)^2} + \frac{\Delta + G\bar{x} - \omega}{\frac{\kappa^2}{4} + (\Delta + G\bar{x} - \omega)^2} \right) \delta x(\omega) \\ &\quad + i\hbar G^2 \bar{a}^2 \left(\frac{\kappa/2}{\frac{\kappa^2}{4} + (\Delta + G\bar{x} + \omega)^2} + \frac{\kappa/2}{\frac{\kappa^2}{4} + (\Delta + G\bar{x} - \omega)^2} \right) \delta x(\omega) \end{aligned} \quad (51)$$

The radiation force perturbs the mechanical susceptibility defined in equation 36 according to the following expression:

$$\chi_{eff}^{-1}(\omega) = \chi^{-1}(\omega) + \chi_{opt}^{-1}(\omega) .$$

We define:

$$\chi_{opt}^{-1} \equiv m_{eff}\omega(2\delta\Omega_m(\omega) - i\Gamma_{opt}(\omega)) \quad (52)$$

in such a way that the perturbed susceptibility has the same form of the mechanical susceptibility:

$$\chi_{eff}^{-1}(\omega) = m_{eff}(\Omega_m^2 + 2\omega\delta\Omega_m(\omega) - \omega^2 - i\omega[\Gamma_m + \Gamma_{opt}(\omega)]) . \quad (53)$$

By definition of susceptibility $\chi(\omega) = \delta x(\omega) / \delta F(\omega)$, we can now compare equation 51 and 52, to obtain:

$$\delta\Omega_m(\omega) = g^2 \frac{\Omega_m}{\omega} \left[\frac{\Delta + \omega}{\frac{\kappa^2}{4} + (\Delta + \omega)^2} + \frac{\Delta - \omega}{\frac{\kappa^2}{4} + (\Delta - \omega)^2} \right] \quad (54)$$

$$\Gamma_{opt}(\omega) = g^2 \frac{\Omega_m}{\omega} \left[\frac{\kappa}{\frac{\kappa^2}{4} + (\Delta + \omega)^2} - \frac{\kappa}{\frac{\kappa^2}{4} + (\Delta - \omega)^2} \right] \quad (55)$$

where we have neglected $G\bar{x}$ since it is much smaller than Δ , and we have introduced the relation $\hbar G^2 \bar{a}^2 = 2m_{eff}\Omega_m g^2$. For a high Q mechanical oscillator, it is

3. DECAY OF A THERMOMECHANICAL SQUEEZED STATE

possible to evaluate $\delta\Omega_m(\omega)$ and $\Gamma_{opt}(\omega)$ at the unperturbed oscillation frequency $\omega = \Omega_m$, yielding to:

$$\delta\Omega_m = g^2 \left[\frac{\Delta + \Omega_m}{\frac{\kappa^2}{4} + (\Delta + \Omega_m)^2} + \frac{\Delta + \Omega_m}{\frac{\kappa^2}{4} + (\Delta - \Omega_m)^2} \right] \quad (56)$$

$$\delta\Omega_m = g^2 \left[\frac{\kappa}{\frac{\kappa^2}{4} + (\Delta + \Omega_m)^2} + \frac{\kappa}{\frac{\kappa^2}{4} + (\Delta - \Omega_m)^2} \right] \quad (57)$$

The response of the intracavity field to the change in the mechanical oscillator's position is not instantaneous but it takes to the field approximately the cavity decay time to respond to that change: this is the dynamical back action effect, which changes the mechanical frequency and the mechanical damping, depending on the laser detuning Δ (and as well on the power of the laser). The effective damping is just the sum of the mechanical (unperturbed)damping, and the optical damping:

$$\Gamma_{eff} = \Gamma_m + \Gamma_{opt} .$$

Γ_m is the damping rate, and it effectively couples the oscillator to the environment (thermal bath). In the same way Γ_{opt} couples the oscillator to the optical field. It can be demonstrated that at the thermal equilibrium the effective temperature of the mechanical oscillator is given by:

$$T_{eff} = \frac{\Gamma_m}{\Gamma_m + \Gamma_{opt}} T_{env} \quad (58)$$

The effective temperature is therefore a function of the laser detuning Δ and can be changed by changing this value. This is known as optomechanical cooling.

3.4 Optical setup

Now that we have given an explanation about how to generate a thermally squeezed state, we will deal with the actual experiment. In figure 19 is shown the optical line used in this experiment.

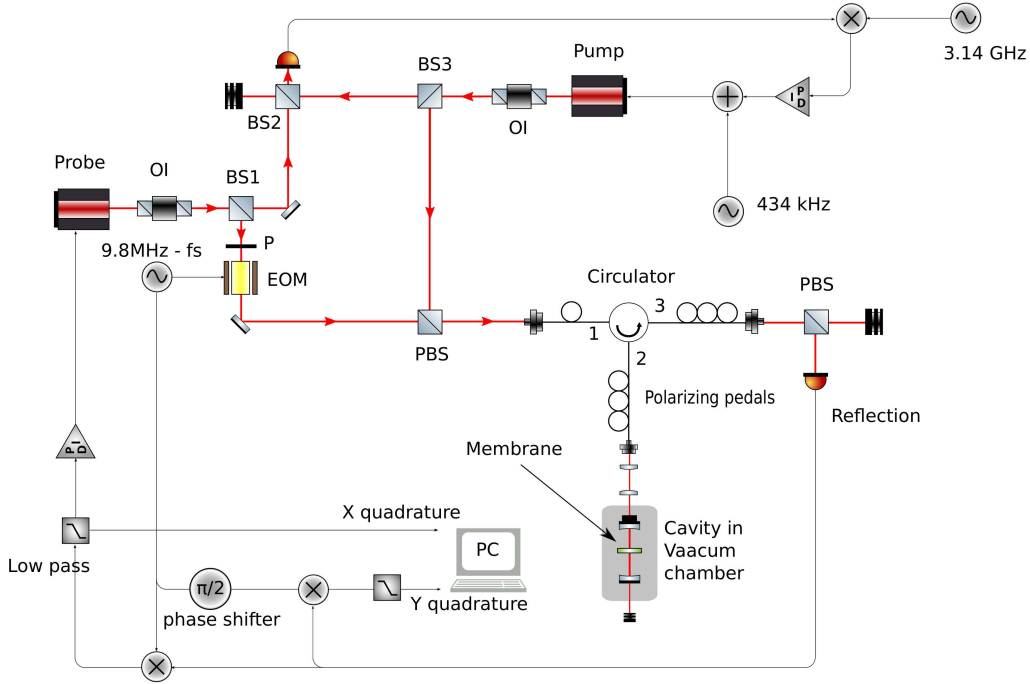


Figure 19: Setup used to study the decay of a squeezed state

It consists of 2 lasers, that we will call probe and pump. The probe laser beam is divided into 2 by the beam splitter placed right after the optical isolator (BS1): one path goes to the cavity and is used to lock the laser's frequency to the cavity with the PDH technique, and the other path goes to another Beam splitter (BS2), where it is mixed with the laser beam coming from the Pump laser. Notice that the PDH method is used for 2 purposes in this experiment: keeping the frequency of the laser locked to the cavity, and for the read-out of the mechanical motion (which will be explained in the following). The Pump laser is used to generate the optical force that allows us to squeeze one of the 2 quadratures. This laser operates 2 free spectral range ($2\text{FSR} \approx 3.14\text{GHZ}$) away from the first laser, in order to avoid unwanted interference. The frequency of this laser is also locked to the cavity by a phase-locked loop that locks its frequency to the frequency of

3. DECAY OF A THERMOMECHANICAL SQUEEZED STATE

the Probe laser. The Pump and Probe laser are mixed in the beam splitter BS2, and the corresponding beating signal is read by a fast photodiode and mixed with an electrical local oscillator operating at $2\text{FSR} \approx 3.14\text{GHZ}$. The output of the mixer has a linear region when the frequency of the Pump laser is very close to the frequency of the Probe laser-2FSR: this output signal will be used as an error signal to keep the laser locked by means of a PID controller. The detuning of the Pump laser from the cavity resonance is monitored using the reflection and transmission signal: while scanning the frequency of the lasers we change the frequency of the Pump laser until the dip of the reflected signal lies in the middle of the beating signal. In this condition the Pump laser is separated exactly by 2FSR from the frequency of the Probe, and as a result we observe that the transmission peak goes at its maximum value. At this point if we want the Pump laser to be detuned with respect to the cavity resonance, we just change the local oscillator frequency. In order to create a squeezed state, we have to parametric modulate the spring constant: this is done using the dynamical backaction effect. The modulation of the frequency of the laser induces a modulation of the frequency shift $\delta\Omega_m$, and of the effective damping Γ_{eff} . The modulation of $\delta\Omega_m$ means modulation of the spring constant, which gives rise to non-zero β in equation 25. We modulated the laser's frequency at $2\Omega_m$ in a region that is red detuned at $-1.43 \times \Omega_m$ with respect to the cavity frequency: this region has been found to be good for squeezing in a previous work carried out in the same research group [12]. Indeed here the slope of $\Gamma_{eff}(\omega)$ is 2.7 times smaller than that of $\delta\Omega_m$, and the effective damping can be treated as a constant: this means that while modulating the laser's frequency we are going to cool down the membrane in a negligible way, and the cooling doesn't depend much on the frequency. The modulation of the frequency of the Pump laser is performed with the aid of an electrical local oscillator. For the read-out of the 2 quadratures we have to demodulate the PDH signal at the mechanical frequency of the mechanical mode we want to squeeze (217 kHz). Since the PDH is obtained by demodulating the reflected signal at 9.88MHz, instead of demodulating again the signal we can demodulate it just one time at a frequency 9.88 MHz+217kHz: in this way we obtain one quadrature. The other quadrature is obtained by introducing a phase shift of $\pi/2$ to the local oscillator before mixing it with the reflected signal read by the photodiode (see the bottom left part of figure 19). Once again we note that the membrane is placed in the middle of the optical cavity. The optical cavity itself is placed inside a vacuum chamber that increase the Q factor of the oscillator (there is no damping due to the air) and isolate the system from noise due to acoustic waves. To this last purpose, the optical cavity is also strongly tightened to the optical table which has a compressed air damping system.

3.5 Experiment and data analysis

In order to measure the decay of a squeezed state, we send a train of pulses to activate the 434 kHz local oscillator that modulates the laser's frequency. Each pulse has a duration of about 10 seconds (during which the frequency is modulated, therefore generating a squeezed state), followed by 3 seconds in which the modulation is switched off. Since the frequency of the (3, 3) mode itself undergoes a drift, every 5 pulses the frequency of the membrane is measured and the local oscillator that modulate the frequency of the laser is adjusted consequently. All the procedure has been automatized, and the whole measurement took few hours. In figure 20 is shown the pulse signal and the two quadratures, acquired as explained in the previous section.

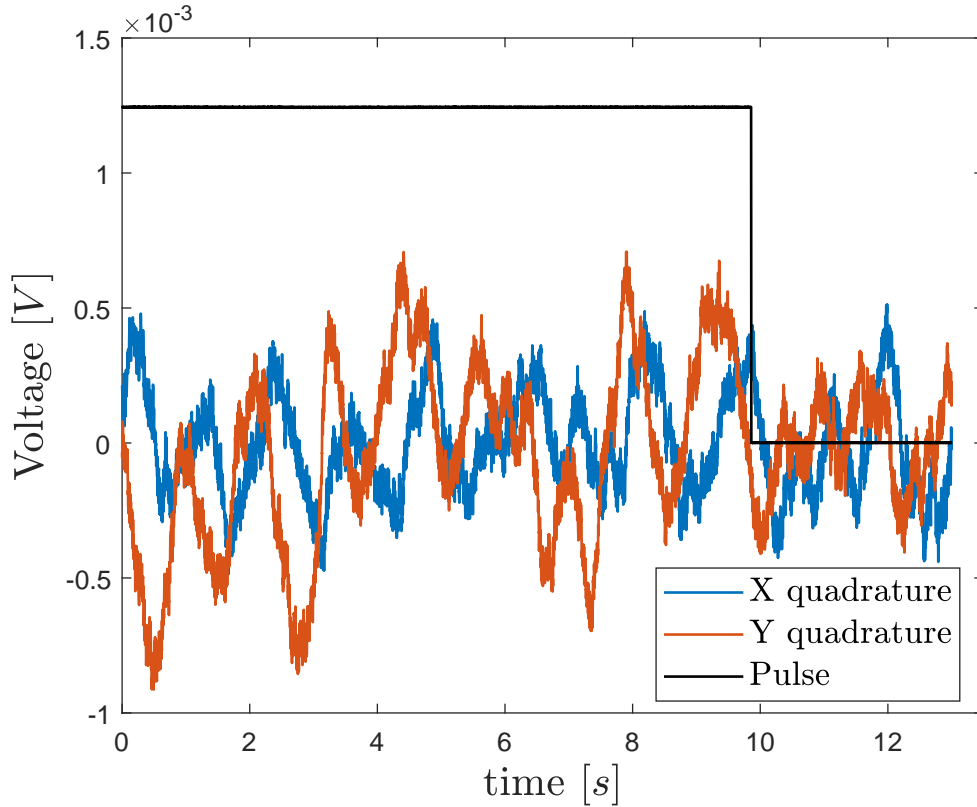


Figure 20: Set of data recorded during the experiment: in black the pulse signal (height has been rescaled to fit in the plot), in blue the X quadrature and in red the Y quadrature. The signal of the two quadratures is given in voltage, and not yet converted into a unit of length (displacement).

We have to make a selection of all the acquired data, because since we were per-

3. DECAY OF A THERMOMECHANICAL SQUEEZED STATE

forming squeezing at the boundaries of the parametric oscillation, for some of the measurements we were driving the membrane. On the other hand in some measurement the squeezing was either not achieved or less strong, due to the drift in the mechanical frequency of the (3, 3) mode: even though every 5 acquisitions we readjusted the modulation frequency to follow the one of the mechanical mode, sometimes the drift was too fast. A squeezed state corresponds to a centered ellipse in the X-Y quadrature plane (see figure 21), but these ellipses are generally not aligned along the X-Y axes because the phase in the demodulation is not set accordingly. Moreover since the frequency of the mechanical mode changes during time, these ellipses rotate at an angular frequency given by the difference between the frequency of the (3, 3) mode and the frequency of the demodulation. Therefore we first adjusted the rotation angle of every measurement, by selecting (for every pulse) just the data lying in the squeezing pulse (roughly the first 10 seconds in figure 20), and fitting the direction of the ellipse. At this point we need to perform the actual selection, to keep only the data squeezed with the same normalized gain parameter g (a compromise has to be done between having states squeezed with the same strength and having a decent number of datasets that allow us to perform a statistical analysis of the data). For this purpose, defining $\Delta X = X_{max} - X_{min}$ and $\Delta Y = Y_{max} - Y_{min}$, after a preliminar look at the data we noticed that the squeezed states had $\Delta X \leq 1.2mV$ and $\Delta Y \geq 1.7mV$. Therefore we applied this condition to keep only data consistent with each other. In order to neglect the driven states (in which the ellipse is not centered in the origin of the X-Y plane), we also applied the condition $R \leq 2mV$, where $R = \langle \sqrt{X^2 + Y^2} \rangle$ and the average is done over all the point in a single dataset (pulse). After this selection we are left with 70 datasets of 700 initial ones.

Since we want to study the decay of the squeezed state, we have to divide the last 3 seconds of each acquisition into smaller time steps, and averaging them over all the different datasets. We don't know what is going to happen, and it can be that the time step required to observe the decay is so small that even if we average over all the different runs, we can't see it. We therefore want to be sure that dividing the data into this timestep, we are able to see the squeezed state if it is there. To this purpose, once again we consider the first 10 seconds of each run since we are sure that there is squeezing here. Mediating over all the datasets, we calculated the variances of the X and Y quadrature, obtaining the following values:

$$\begin{aligned}\langle X^2 \rangle_{total} &= (2.5 \pm 0.3) \times 10^{-8}V \\ \langle Y^2 \rangle_{total} &= (4.9 \pm 0.8) \times 10^{-7}V\end{aligned}$$

In order to check if we can see a squeezed state considering a time step smaller than the 10 seconds, we divided the total run time into increasingly smaller time bins, calculating for each one the variances and checking if the distribution (after

3. DECAY OF A THERMOMECHANICAL SQUEEZED STATE

mediating over all the datasets) was still Gaussian. As a criterium to decide whether we can still see the squeezed state, we checked if the variances were lying in the following intervals:

$$\langle X^2 \rangle_{small} \in [\langle X^2 \rangle_{total} \pm k\sigma_{\langle X^2 \rangle}]$$

$$\langle Y^2 \rangle_{small} \in [\langle Y^2 \rangle_{total} \pm k\sigma_{\langle Y^2 \rangle}]$$

where k is a cover factor arbitrarily set to 3, and $\sigma_{\langle X^2 \rangle}$, $\sigma_{\langle Y^2 \rangle}$ are the standard uncertainties on $\langle X^2 \rangle_{total}$ and $\langle Y^2 \rangle_{total}$. The minimum time bin found such that these criteria are satisfied is $\Delta t \approx 70\mu s$, and we are sure that dividing the data into time steps of this length (and averaging over all the datasets), we are able to see the squeezed state, if it is present.

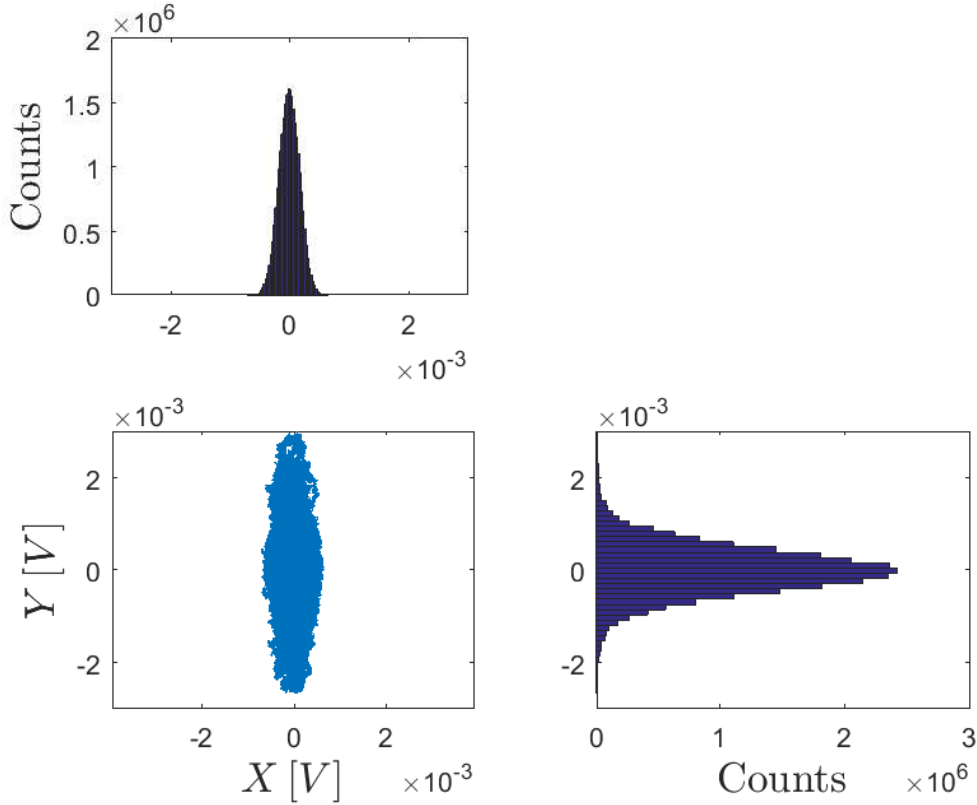


Figure 21: In figure is shown the ellipse corresponding to the squeezed quadrature. The histograms of the quadratures show how the Gaussian distribution has a different variance along the 2 quadratures.

In figure 21 is shown the squeezed state in the X-Y quadrature plane, and the histograms corresponding to the X and Y quadratures. The variances of the 2

3. DECAY OF A THERMOMECHANICAL SQUEEZED STATE

quadratures are $\langle X^2 \rangle_{total}$ and $\langle Y^2 \rangle_{total}$ given before, and according to equations 32 this corresponds to a normalized gain parameter $g=0.90$.

Now we can analyze the data: by dividing every dataset into time-steps of $\Delta t \approx 16ms$, and merging the data from the different datasets that correspond to the same time bin, we are able to calculate the variance of the X and Y quadrature as a function of time. The result is shown in figure 22.

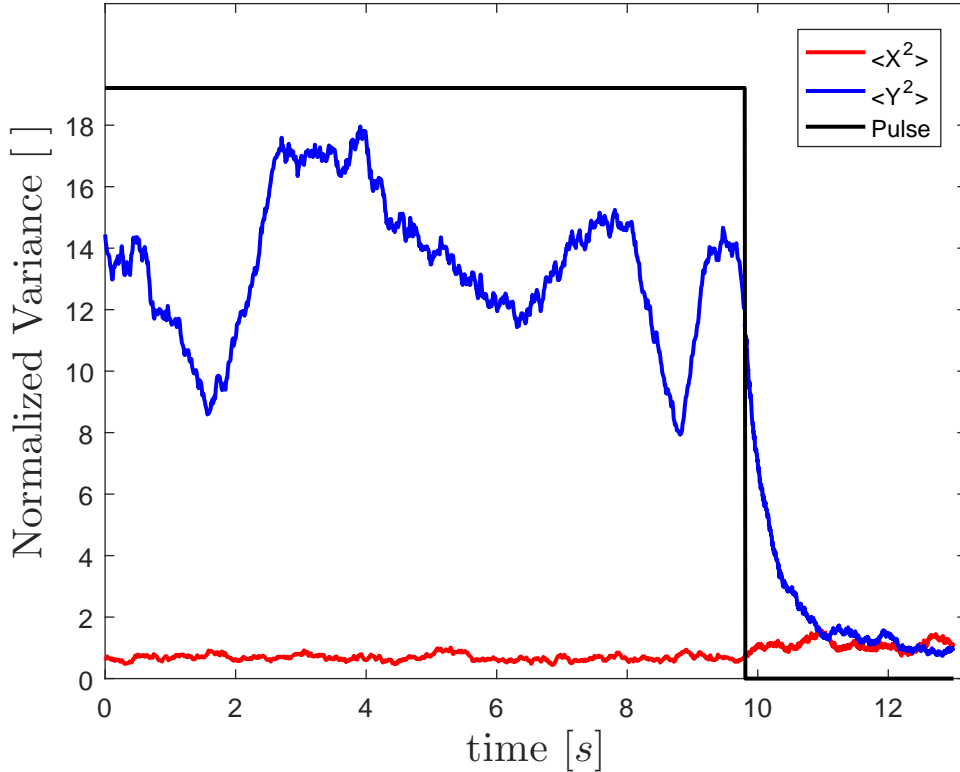


Figure 22: In red and blue are shown the Variances of the Y and X quadratures, normalized by the variance of the thermal distribution (i.e without squeezing). The black line is the pulse signal: when high the modulation of the spring constant is on, when low the spring constant is not modulated.

Notice that right after the frequency modulation was stopped (see the black pulse signal in the figure), the ellipse in the quadratures plane started rotating over time and therefore in order to obtain the plot of figure 22, this rotation has been corrected. Looking at the picture we can infer few things: first of all if we consider the first 9.8 seconds (during which parametric modulation of the optical spring is on), the variance of the Y quadrature is much more unstable than the one of the X quadrature. This is due because we are operating at the boundary of the

3. DECAY OF A THERMOMECHANICAL SQUEEZED STATE

3dB limit: near this area the normalized gain parameter approaches to 1, which is a discontinuity point for the Y variance, while it isn't for the X variance (see equations 32). As a consequence, the sensitivity of $\langle Y^2 \rangle$ over a small change of g is much higher than for the X quadrature: $\delta \langle Y^2 \rangle / \delta g \gg \delta \langle X^2 \rangle / \delta g$. Another reason that affect the instability of the variances is the number of datasets over which we are performing the measurements: the higher number of data we have in the bidimensional Gaussian distribution (the ellipse), the lower the error on its variance. As explained before while discussing how the data were filtered, these 2 factors are in competition: if we want g to be the same for all the acquisitions, then we have to discard a lot of measurements and we will be left with few datasets. Now we focus the analysis on what happens after we switch off the modulation. As it can be seen in figure 22, the variance of the Y quadrature decays to a baseline level. On the other hand, by looking at the squeezed quadrature we see that its value increases, but we can not really see a clear decay since the data are very noisy. Notice that in this case the noise is only due to the statistical error due to low number of dataset used (the noise due to variation in g is not present here since we are not modulating the spring constant). By fitting $\langle Y^2 \rangle$ with an exponential function $\langle Y^2 \rangle = Y_0 + Ae^{-t/\tau}$, we obtain the following time constant for the decay of the heated quadrature:

$$\tau_{decay} = (0.39 \pm 0.01) s .$$

In figure 23 are shown the variances of the quadratures after the modulation of the spring constant is switched off. In black there is the fitting equation for $\langle Y^2 \rangle$. As mentioned before, the ellipses in the quadrature plane not only started to decay to the thermal distribution, but also started rotating. In figure 23 are also shown the ellipses at different point in time. Notice that for the calculation of the X, Y variances the rotation has been corrected.

Unfortunately the decay of the X quadrature can not be seen, since the statistical error is too high and the variance of the squeezed quadrature is just about 2 times smaller than in case of non-squeezing. In figure 22 can be seen that the final baseline value for $\langle X^2 \rangle$ in the non-squeezed area is higher than the baseline value it has during the squeezing. But due to the statistical error in the calculation of the variance, we are not able to clearly see a decay.

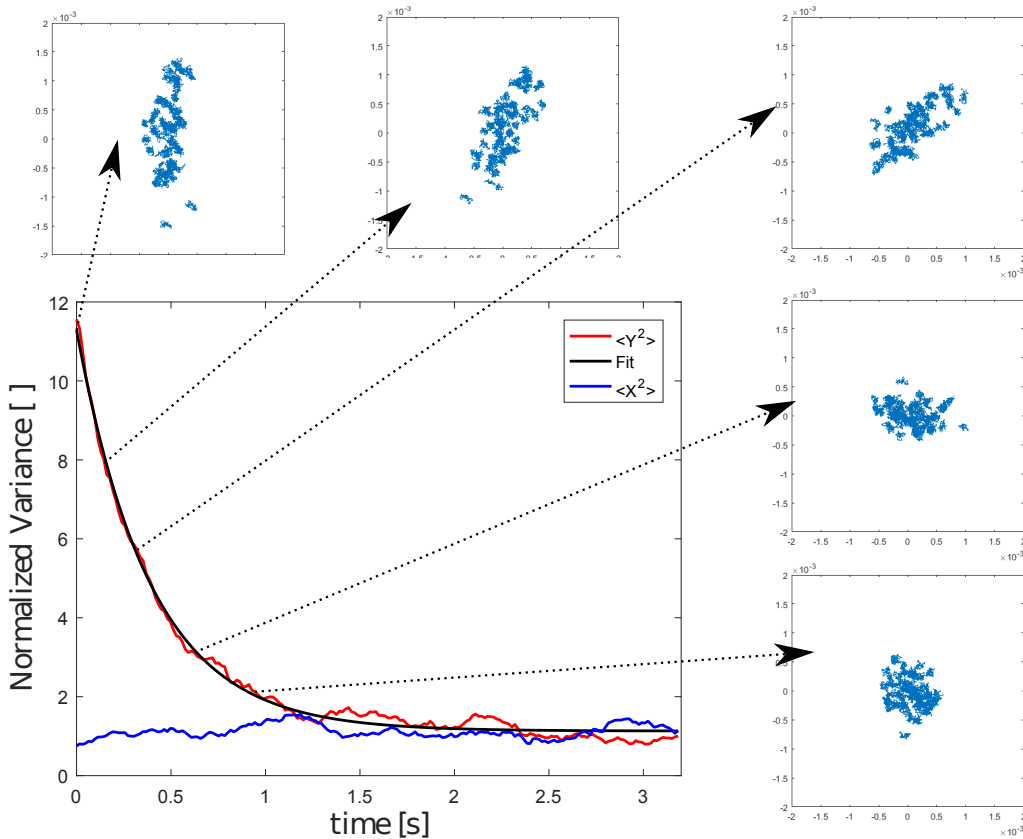


Figure 23: The plot shows the time evolution of the the X and Y quadratures from a squeezed state to a non squeezed one. The blue and red lines are the normalized variances respectively of the X and Y quadratures (i.e variance of the quadrature divided the variance of the non-squeezed state). The black line is the fitting function for the Y quadrature: $\langle Y^2 \rangle = Y_0 + Ae^{-t/\tau}$, with a fitted decay time $\tau_{decay} = (0.39 \pm 0.01) s$. In the same figure are also shown the distributions of the quadratures in the XY plane, at different times ($t_1 = 0s, t_2 = 0.16s, t_3 = 0.32s, t_4 = 0.64s, t_5 = 0.96s$). In this distributions is visible a rotation, that has been corrected to create the plot of the variances over time.

3.6 Conclusions and future developements

During this thesis work there wasn' t enough time to perform further measurements, but here we give some indications (for future measurements) on how to solve the problems encountered. The simplest thing to do is to increase the number of data acquisitions, in order to increase the statistics and have a lower statistical error on the measurement: this should allow to see the decay also for the X quadrature. However the number of dataset can be increased only to some extent, since the amount of data per dataset is really high, and already for the number

3. DECAY OF A THERMOMECHANICAL SQUEEZED STATE

of datasets used in this experiments the software for the data analysis takes a lot of time to perform the calculations. A more clever solution to apply together with the previous one is to surpass the 3dB squeezing limit. This can be done by applying a feedback mechanism that cools the heated quadrature (Y) in such a way that it doesn't diverge. This has two big advantages: first of all the sensitivity $\delta \langle Y^2 \rangle / \delta g$ is reduced (for the same squeezing strength), allowing to have more states squeezed with the same strength, and reducing the number of dataset to be discarded. The second important advantage is that we can squeeze the X quadrature more and in such a way we are going to make it easier to distinguish the decay from the noise in the data, since we effectively increased the gap between the variance of the squeezed state, and the variance of the non-squeezed one. We started this investigation with the purpose to find out how a squeezed state goes back to a non-squeezed one, and to see if in the future it will be possible to transfer a thermally squeezed state between two different modes of the mechanical oscillator. To our knowledge, this is the first time that the measurement of the decay of a thermally squeezed state is performed, and even though we couldn't measure it for both the quadratures, we got a time decay constant for one of them. The methods previously suggested to measure also the decay of the X quadrature, could deal to interesting results and to the definitive answer to the questions that arised and motivated this investigation.

Bibliography

- [1] Markus Aspelmeyer, Tobias J. Kippenberg, and Florian Marquardt. Cavity Optomechanics. *Reviews of Modern Physics*, 86(4):1391–1452, December 2014.
- [2] Bahaa E. A. Saleh and Malvin Carl Teich. *Fundamentals of Photonics*. 1991.
- [3] Peter E. Bradley and Ray Radebaugh. Properties of Selected Materials at Cryogenic Temperatures — NIST. *CRC Handbook of Chemistry and Physics*, June 2013.
- [4] Robert J Corruccini and John J Gniewek. Thermal expansion of technical solids at low temperatures; a compilation from the literature. Technical Report NBS MONO 29, National Bureau of Standards, Gaithersburg, MD, 1961.
- [5] Bradley J. Frey and Douglas B. Leviton. Automation, operation, and data analysis in the cryogenic, high accuracy, refraction measuring system (CHARMS). In James B. Heaney and Lawrence G. Burriesci, editors, *Optics & Photonics 2005*, page 59040P, San Diego, California, USA, August 2005.
- [6] Bradley J. Leviton Frey. Cryogenic Temperature-dependent Refractive Index Measurements of N-BK7, BaLKN3, and SF15 for NOTES PDI. In *SPIE Optics and Photonics*, San Diego, CA, United States, January 2007.
- [7] J. H. Burge, T. Peper, and S. F. Jacobs. Thermal Expansion of Borosilicate Glass, Zerodur, Zerodur M, and Uncer amized Zerodur at Low Temperatures. *Applied Optics*, 38(34):7161–7162, December 1999.
- [8] T P Purdy, R W Peterson, P-L Yu, and C A Regal. Cavity optomechanics with Si_3N_4 membranes at cryogenic temperatures. *New Journal of Physics*, 14(11):115021, November 2012.
- [9] R. W. P. Drever, J. L. Hall, F. V. Kowalski, J. Hough, G. M. Ford, A. J. Munley, and H. Ward. Laser phase and frequency stabilization using an optical resonator. *Applied Physics B Photophysics and Laser Chemistry*, 31(2):97–105, June 1983.
- [10] Eric D. Black. An introduction to Pound–Drever–Hall laser frequency stabilization. *American Journal of Physics*, 69(1):79–87, December 2000.
- [11] M Nickerson. A review of Pound-Drever-Hall laser frequency locking. page 11.

- [12] Sameer Sonar, Vitaly Fedoseev, Matthew J. Weaver, Fernando Luna, Elger Vlieg, Harmen van der Meer, Dirk Bouwmeester, and Wolfgang Löffler. Strong thermomechanical squeezing in a far-detuned membrane-in-the-middle system. *Physical Review A*, 98(1):013804, July 2018.
- [13] Andrea Vinante and Paolo Falferi. Feedback-enhanced parametric squeezing of mechanical motion. *Physical Review Letters*, 111(20):207203, November 2013.
- [14] F. M. Buters, Science, and Leids Instituut Onderzoek Natuurkunde. Where photons meet phonons. <https://openaccess.leidenuniv.nl/handle/1887/58471>, December 2017.
- [15] Ermanno F. Borra. The art of cryogenic lens design: The Gemini Planet Imager. 2010.
- [16] Masud Mansuripur. The Ewald–Oseen Extinction Theorem. page 17.
- [17] A. Pontin, M. Bonaldi, A. Borrielli, F. S. Cataliotti, F. Marino, G. A. Prodi, E. Serra, and F. Marin. Squeezing a thermal mechanical oscillator by stabilized parametric effect on the optical spring. *Physical Review Letters*, 112(2):023601, January 2014.
- [18] D. Rugar and P. Grütter. Mechanical parametric amplification and thermomechanical noise squeezing. *Physical Review Letters*, 67(6):699–702, August 1991.
- [19] Phys. Rev. Lett. 67, 699 (1991) - Mechanical parametric amplification and thermomechanical noise squeezing. <https://journals.aps.org/prl/abstract/10.1103/PhysRevLett.67.699>.
- [20] A. M. Jayich, J. C. Sankey, B. M. Zwickl, C. Yang, J. D. Thompson, S. M. Girvin, A. A. Clerk, F. Marquardt, and J. G. E. Harris. Dispersive optomechanics: A membrane inside a cavity. *New Journal of Physics*, 10(9):095008, September 2008.
- [21] Kyungwon An, Changhui Yang, Ramachandra R. Dasari, and Michael S. Feld. Cavity ring-down technique and its application to the measurement of ultraslow velocities. *Optics Letters*, 20(9):1068, May 1995.